

THE SLOAN LENS ACS SURVEY. III – THE STRUCTURE AND FORMATION OF  
 EARLY-TYPE GALAXIES AND THEIR EVOLUTION SINCE  $Z \approx 1$

LÉON V.E. KOOPMANS<sup>1</sup>, TOMMASO TREU<sup>2</sup>, ADAM S. BOLTON<sup>3,5</sup>, SCOTT BURLES<sup>3</sup> AND LEONIDAS A. MOUSTAKAS<sup>4</sup>  
*Accepted by ApJ*

ABSTRACT

We present a joint gravitational lensing and stellar dynamical analysis of fifteen massive field early-type galaxies – selected from the *Sloan Lens ACS* (SLACS) Survey – using *Hubble Space Telescope* ACS images and luminosity weighted stellar velocity dispersions obtained from the Sloan Digital Sky Survey database. The sample of lens galaxies is well-defined (see Paper I), with a redshift range of  $z=0.06-0.33$  and an average stellar velocity dispersion of  $\langle\sigma_{\text{ap}}\rangle = 263 \text{ km s}^{-1}$  (rms of  $44 \text{ km s}^{-1}$ ) inside a 3-arcsec fiber diameter. The following numerical results are found: (i) A joint-likelihood gives an average logarithmic density slope for the *total* mass density of  $\langle\gamma'\rangle = 2.01_{-0.03}^{+0.02}$  (68% C.L.;  $\rho_{\text{tot}} \propto r^{-\gamma'}$ ) inside  $\langle R_{\text{Einst}}\rangle = 4.2 \pm 0.4 \text{ kpc}$  (rms of  $1.6 \text{ kpc}$ ). The inferred *intrinsic* rms spread in logarithmic density slopes is  $\sigma_{\gamma'} = 0.12$ , which might still include some minor systematic uncertainties. A range for the stellar anisotropy parameter  $\beta = [-0.25, +0.25]$  results in  $\Delta\langle\gamma'\rangle = [+0.05, -0.09]$ . Changing from a Hernquist to a Jaffe luminosity density profile increases  $\langle\gamma'\rangle$  by 0.05. (ii) The average position-angle difference between the light distribution and the total mass distribution is found to be  $\langle\Delta\theta\rangle = 0 \pm 3$  degrees (rms of 10 degrees), setting an upper limit of  $\langle\gamma_{\text{ext}}\rangle \lesssim 0.035$  on the average external shear. The total mass has an average ellipticity  $\langle q_{\text{SIE}}\rangle = 0.78 \pm 0.03$  (rms of 0.12), which correlates extremely well with the stellar ellipticity,  $q_*$ , resulting in  $\langle q_{\text{SIE}}/q_*\rangle = 0.99 \pm 0.03$  (rms of 0.11) for  $\sigma \gtrsim 225 \text{ km s}^{-1}$ . At lower velocity dispersions, inclined S0 galaxies dominate, leading to a higher ratio (up to 1.6). This suggests that the dark-matter halo surrounding these galaxies is less flattened than their stellar component. Assuming an oblate mass distribution and random orientations, the distribution of ellipticities implies  $\langle q_3 \rangle \equiv \langle (c/a)_\rho \rangle = 0.66$  with an error of  $\sim 0.2$ . (iii) The average projected dark-matter mass fraction is inferred to be  $\langle f_{\text{DM}} \rangle = 0.25 \pm 0.06$  (rms of 0.22) inside  $\langle R_{\text{E}} \rangle$ , using the stellar mass-to-light ratios derived from the Fundamental Plane as priors. (iv) Combined with results from the *Lenses Structure & Dynamics* (LSD) Survey at  $z \gtrsim 0.3$ , we find no significant evolution of the total density slope inside one effective radius for galaxies with  $\sigma_{\text{ap}} \geq 200 \text{ km s}^{-1}$ : a linear fit gives  $\alpha_{\gamma'} \equiv d\langle\gamma'\rangle/dz = 0.23 \pm 0.16$  ( $1\sigma$ ) for the range  $z=0.08-1.01$ . We conclude that massive early-type galaxies at  $z=0.06-0.33$  on average have an isothermal logarithmic density slope inside half an effective radius, with an intrinsic spread of at most 6% ( $1\sigma$ ). The small scatter and absence of significant evolution in the inner density slopes suggest a collisional scenario where gas and dark matter strongly couple during galaxy formation, leading to a total mass distribution that rapidly converge to dynamical *isothermality*.

*Subject headings:* gravitational lensing — galaxies: elliptical and lenticular, cD — galaxies: evolution — galaxies: formation — galaxies: structure

1. INTRODUCTION

Massive early-type galaxies are postulated to be late-comers in the hierarchical formation process (e.g. Blumenthal et al. 1984; Frenk et al. 1985), formed via mergers of lower-mass (disk) galaxies (e.g. Toomre & Toomre 1972; Schweizer 1982; Frenk et al. 1988; White & Frenk 1991; Barnes 1992; Cole et al. 2000). As such, a detailed study of their structure (e.g. Navarro, Frenk & White 1996; Moore et al. 1998), formation and subse-

quent evolution provides a powerful test of the concordance  $\Lambda$ CDM paradigm (e.g. Riess et al. 1998; Perlmutter et al. 1999; Spergel et al. 2003; Tegmark et al. 2004) at galactic scales.

In this context, the merging of low-mass galaxies to form more massive ones naively seems to imply a continuous evolution of their mass structure (e.g. Bullock et al. 2001), both in their outer regions and dense inner regions (e.g. smaller galaxies accrete and sink to the center through dynamical friction). On the one hand, the inner regions of massive ellipticals can contract into an increasingly denser structure, if significant mass in dissipational gas is accreted (e.g. Blumenthal et al. 1986; Ryden & Gunn 1987; Navarro & Benz 1991; Dubinski 1994; Jesseit, Naab & Burkert 2002; Gnedin et al. 2004; Kazantzidis et al. 2004). If this process occurs at  $z \lesssim 1$  (e.g. Kauffmann, Charlot & White 1996; Kauffmann & Charlot 1998) and results in star-formation activity, one can test this scenario directly by using high-quality data of early-type galaxies, obtained with space

<sup>1</sup> Kapteyn Astronomical Institute, University of Groningen, P.O.Box 800, 9700 AV Groningen, The Netherlands (koopmans@astro.rug.nl)

<sup>2</sup> Department of Physics, University of California, Santa Barbara, CA 93106, USA (ttreu@physics.ucsb.edu)

<sup>3</sup> Department of Physics and Kavli Institute for Astrophysics and Space Research, Massachusetts Institute of Technology, 77 Massachusetts Ave., Cambridge, MA 02139, USA (burles@mit.edu)

<sup>4</sup> Jet Propulsion Laboratory, Caltech, MS 169-327, 4800 Oak Grove Dr., Pasadena, CA 91109 (leonidas@jpl.nasa.gov)

<sup>5</sup> Harvard-Smithsonian Center for Astrophysics, 60 Garden St. MS-20, Cambridge, MA 02138 USA (abolton@cfa.harvard.edu)

and 8–10 m class ground-based telescopes (e.g. Menanteau et al. 2001a&b; Gebhardt et al. 2003; McIntosh et al. 2005; Tran et al. 2005). On the other hand, the mass inside the inner  $\sim 10$  kpc of the most massive ellipticals (i.e.  $>L_*$ ) seems to remain nearly constant from  $z \gg 1$  to the present day – as suggested by collisionless dark-matter simulations – and additionally accreted dark matter replaces already-present collisionless matter (e.g. Wechsler et al. 2002; Zhao et al. 2003; Gao et al. 2004). If most gas is turned into (collisionless) stellar mass before mergers (e.g. van Dokkum et al. 1999), one expects it to behave similarly to dark matter during assembly in to the more massive galaxies seen at  $z \lesssim 1$ .

Based on the notion that the velocity function of massive early-type galaxies at  $z=0$  (Sheth et al. 2003) is remarkably close to that of the inner regions (inside  $\sim 10$  kpc) of the most massive simulated galaxies at  $z \approx 6$  – even though these galaxies continue to accrete collisionless matter below that redshift – Loeb & Peebles (2003) suggest that the inner regions might behave as *dynamical attractors*, whose phase-space density is nearly invariant under the accretion of collisionless matter (see also e.g. Gao et al. 2004; Kazantzidis, Zentner & Kravtsov 2005). In this scenario, one might expect less structural evolution of the inner regions of massive early-type galaxies at  $z < 1$ , compared to models where most gas had not yet turned into stars *before* the mass assembly of their inner regions took place. Hence, one way to study the formation scenario of massive ellipticals, is to quantify the evolution of the mass distribution in their inner regions from redshifts  $z=1$  to 0.

From the observational point of view, a significant effort has been devoted in the past two decades to the study of the mass structure of early-type galaxies in the local Universe ( $z \lesssim 0.1$ ) through stellar dynamical tracers and X-ray studies (e.g. Fabbiano 1989; Mould et al. 1990; Matsushita et al. 1998; Loewenstein & White 1999; Saglia et al. 1992; Bertin et al. 1994; Arnaboldi et al. 1996; Franx et al. 1994; Carollo et al. 1995; Rix et al. 1997; Gerhard et al. 2001; Seljak 2002; Borriello et al. 2003; Romanowsky et al. 2003). In a comprehensive study, Gerhard et al. (2001) conclude that massive ellipticals have, on average, flat circular velocity curves with a scatter of  $\sim 10\%$  in their inner two effective radii. This in itself should impose stringent constraints on any numerical simulations of elliptical galaxies (e.g. Meza et al. 2003; Kawata & Gibson 2003).

Strong gravitational lensing provides a complementary approach (Kochanek 1991) to study early-type galaxies at higher redshifts. Lensing analysis has been used to demonstrate the presence of dark matter around early-type galaxies and, in some systems, to provide evidence for “isothermal” (i.e.  $\rho_{\text{tot}} \propto r^{-2}$ ) mass density profiles equivalent to the flat rotation curves observed for spiral galaxies (e.g., Kochanek 1995; Rusin & Ma 2001; Ma 2003; Rusin et al. 2002, 2003a; Cohn et al. 2001; Munoz et al. 2001; Winn et al. 2003; Wucknitz et al. 2004; Rusin & Kochanek 2005). However, the mass-profile (e.g. Wucknitz 2002) and mass-sheet degeneracies (Falco et al. 1985) often prevent a truly accurate determination of the logarithmic density slope *at* the Einstein radius.

To answer the question “*What is the mass structure inside the inner regions of early-type galaxies and how does it evolve with time?*”, we therefore combine constraints

from strong gravitational lensing and stellar kinematics. The former provides an accurate mass measurement inside the Einstein radius (Kochanek 1991), whereas the latter provides a measurement of the mass gradient. The average logarithmic density slope inside the Einstein radius can then be determined – independent of the mass-sheet degeneracy that is associated with the galaxy mass distribution – with the same fractional accuracy as is obtained on the luminosity-weighted stellar velocity dispersion (e.g. see Treu & Koopmans 2002 and Koopmans 2004). The density slopes of *individual* early-type galaxy can be correlated with redshift, to determine any structural evolution in the population.

In an ongoing study of massive early-type lens galaxies between  $z \approx 0.5$  and 1, as part of the *Lenses Structure & Dynamics* (LSD) Survey (Koopmans & Treu 2002, 2003; Treu & Koopmans 2002, 2003, 2004; hereafter TK04) – plus two additional systems that were studied to measure the Hubble Constant (Treu & Koopmans 2002; Koopmans et al 2003) – this technique has successfully been applied, to place the first constraints on the inner density slopes and dark-matter halos of early-type galaxies to  $z \approx 1$  (TK04), finding a logarithmic density slope close to isothermal, although the results were limited by the small sample size.

In the first paper of this series (Bolton et al. 2006; hereafter Paper I), we reported on the discovery of nineteen new early-type lens galaxies from the *Sloan Lens ACS* (SLACS) Survey at  $z \lesssim 0.3$ , each with *Hubble Space Telescope* (HST) F435W and F814W images and a stellar velocity dispersion measured from their SDSS spectra (e.g. Bolton et al. 2004). Some systems have integral field spectroscopy (IFS) of their lensed sources, obtained with Magellan and/or Gemini (see also Bolton et al. 2005). As far as their photometric properties are concerned, they are representative of Luminous Red Galaxies (LRG; Eisenstein et al. 2004) with similar redshifts and similar stellar velocity dispersions (see Paper I). They also lie on the Fundamental Plane (FP; Dressler et al. 1987; Djorgovski & Davis 1987) of early-type galaxies, have old stellar populations, and have very homogeneous mass density profiles (Treu et al. 2006; hereafter Paper II).

In this paper, we focus on the analysis of a sub-sample of fifteen isolated early-type lens galaxies from SLACS, combining the constraints from *Hubble Space Telescope* (HST) images with the stellar velocity dispersion obtained from the SDSS database. The goals are to quantify their inner mass structure and to assess whether any evolution of their inner regions has occurred at  $z \lesssim 1$ . In §2, we present non-parametric lens models for each system. The simplicity of the models supports their lensed nature and provides the necessary input for subsequent analysis. In §3, we use the enclosed mass from lensing in a joint stellar-dynamical analysis, to determine the inner density slopes of each early-type galaxy. In combination with results from the LSD survey, we analyze the redshift behavior of the density slope in §4 to quantify its evolution. In §5, we summarize our results and draw conclusions. Throughout this paper, we assume  $H_0 = 70 \text{ km s}^{-1} \text{ Mpc}^{-1}$ ,  $\Omega_m = 0.3$  and  $\Omega_\Lambda = 0.7$ .

## 2. GRAVITATIONAL-LENS MODELS

In this section, we briefly summarize the selection procedure of lens candidates for the HST snapshot program

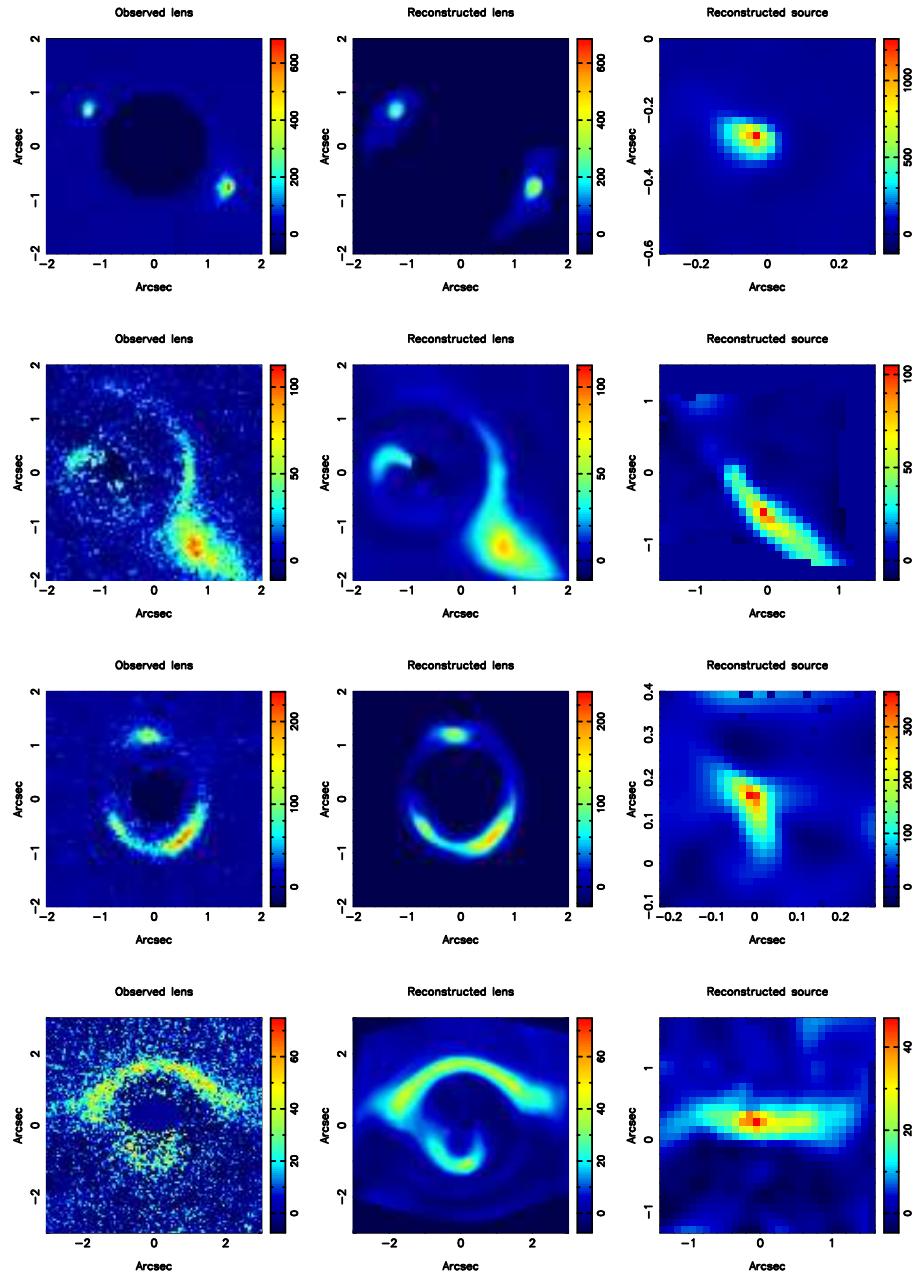


FIG. 1.— Non-parametric lens-image reconstructions of confirmed SLACS lens systems. For each system, the observed (galaxy-subtracted) HST-ACS F814W image is shown (left panel), the best reconstruction of the system (middle panel) and source model (right panel), assuming a SIE mass model. From top to bottom are shown: J0037–0942, J0216–0813, J0737+3216, and J0912+0029 (see Paper I and Table 1).

(see Bolton et al. 2004 and Paper I) and the sub-sample of the fifteen early-type lens galaxies that we use throughout this paper, in addition to their lens models. The models are used to quantify the alignment between stellar and total mass (§ 2.4) and provide the mass enclosed by the lensed images as an external constraint on the stellar-dynamical models (§ 3).

### 2.1. The Sample

The selection procedure that led to the current sample of confirmed E/S0 lens galaxies, used in this paper, is as follows: first, a principle-component analysis (PCA) is

done of all spectra in the LRG and MAIN galaxy samples from the SDSS. The smooth PCA spectra are subtracted from the observed spectra and the residuals are studied for absorption and higher-redshift emission lines. The absorption lines secure the redshift of the foreground galaxy and allow the luminosity-weighted stellar velocity dispersions to be measured for the brighter galaxies. Second, the residual spectra that show three or more atomic transition lines in emission, including [O II], at a single redshift beyond that of the main galaxy are selected for follow-up. Third, given the redshifts and stellar velocity dispersions ( $\sigma_{\text{ap}}$ ) of the foreground galaxies, and the

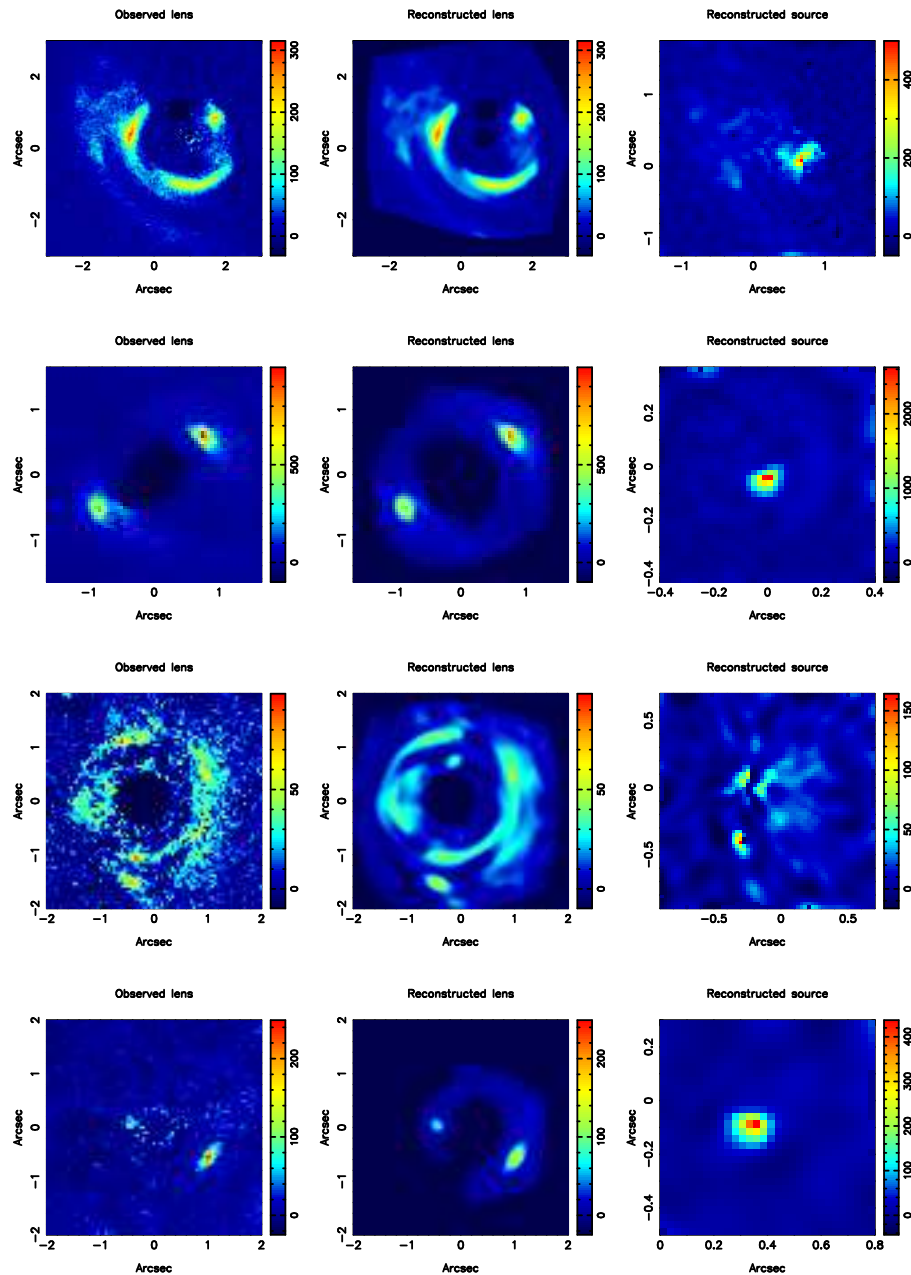


FIG. 1.— (Continued) From top to bottom are shown: J0956+5100, J0959+0410, J1250+0523 and J1330-0148.

redshifts of the lensed source candidates, we can estimate their lensing probability by ranking the systems according to their Einstein radii  $\theta_E = 4\pi(\sigma_{\text{ap}}/c)^2 D_{\text{ds}}/D_s$ , assuming a SIS mass model with  $\sigma_{\text{SIS}} \equiv \sigma_{\text{ap}}$  (e.g. Schneider et al. 1992) from large to small<sup>6</sup>. This procedure resulted in a ranked list of 49 candidates, of which 20 are from the LRG sample in Bolton et al. (2004) and the remaining

<sup>6</sup> Note that in the context of the SIS model, all systems with  $2\theta_E \geq 1.5''$  (the SDSS fiber radius) have a probability of unity to be multiply imaged lens systems, because one of the two lensed images forms between  $0-1\theta_E$  and the second image forms between  $1-2\theta_E$ . Hence, observing an image inside  $2\theta_E$  implies that a counter image must exist.

29 are from the MAIN galaxy sample. We further note that galaxies in the LRG sample were selected based on early-type spectra, photometry and morphology (Eisenstein et al. 2001), whereas the MAIN sample is more heterogeneous with the general requirement, set by us, that  $\text{EW}_{\text{H}\alpha} < 1.5 \text{ \AA}$  (but see Paper I). Even though the selection is not completely uniform, the resulting sample of E/S0 lens systems is indistinguishable in its photometric and scaling-relation properties from non-lens samples (see Paper II). Nonetheless, we remain cautious of potential selection effects.

Of the 28 systems observed as of 2005 March 31 – the cutoff date for this first series of papers – we confirmed

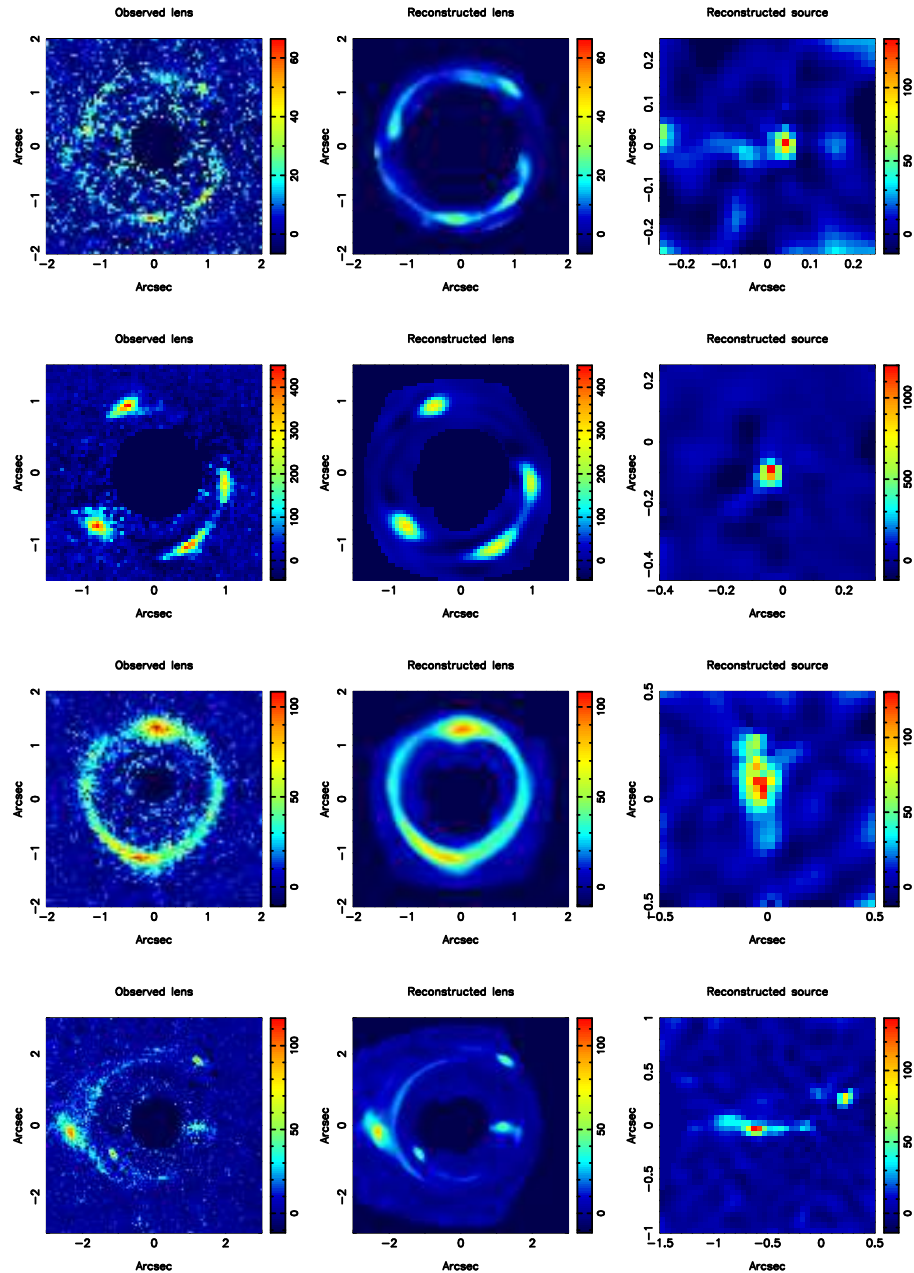


FIG. 1.— (Continued) From top to bottom are shown: J1402+6321, J1420+6019, J1627-0055 and J1630+4520.

19 as unambiguous lens systems. Of the remaining 9 systems, six show some hint of a counter-image near the galaxy center, but in all these cases these are too faint to be confirmed as true lens systems with the present data (Paper I), while three lack any visible lensed images<sup>7</sup> or are magnified, but singly imaged, galaxies inside the SDSS fiber aperture.

The galaxy-subtracted HST-ACS F435W and F814W images of each of the observed SLACS lens candidates are presented in Paper I. In general, the F814W images

<sup>7</sup> Lensed images can still be extended and below the noise level of the shallow Snapshot images.

have better signal-to-noise compared to the F435W images and thus serve as the primary constraint on the lens models. The F435W images are only used to further validate the lensed nature of the multiple images (e.g. based on similar colors and structure).

In this paper, four additional lens systems are removed to construct a clean sample of “isolated” early-type galaxies<sup>8</sup>: one system is a bulge-dominated spiral galaxy

<sup>8</sup> Because massive galaxies preferentially occur in over-dense regions, no truly isolated early-type galaxies exist. We therefore only discard those systems where either the observations or the lens model can significantly be affected by other nearby massive galaxies. In general, the latter means two similar galaxies within

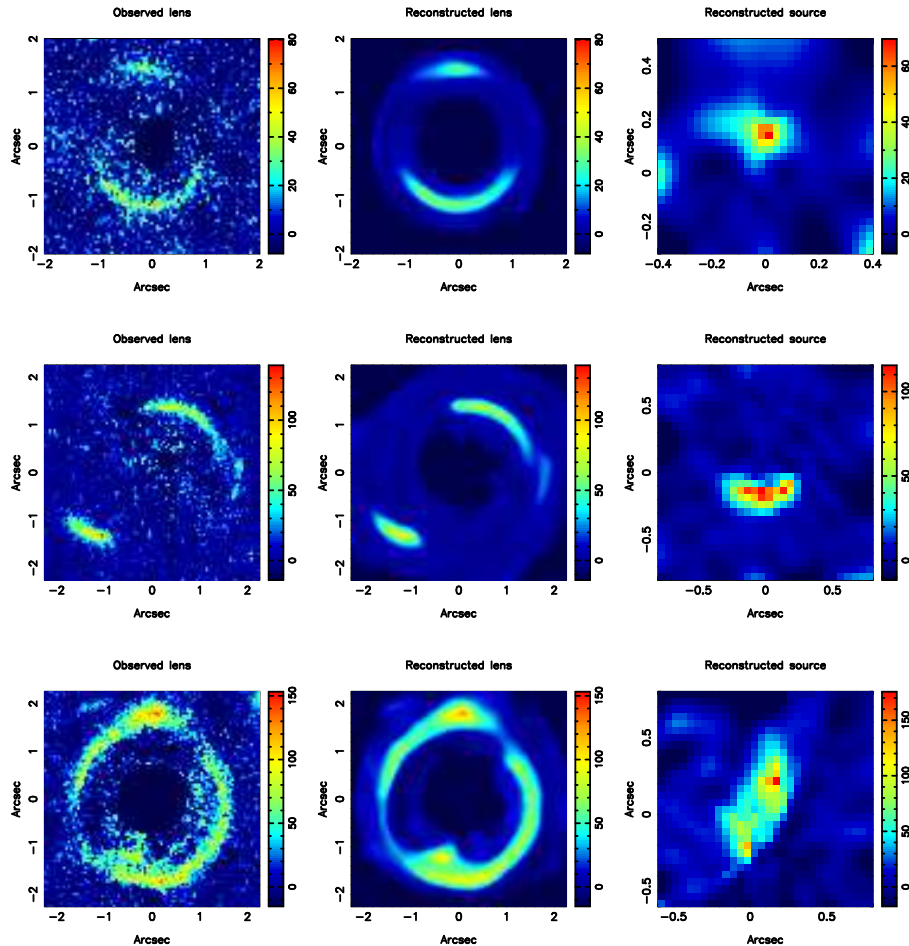


FIG. 1.— (Continued) From top to bottom are shown: J2300+0022, J2303+1422 and J2321-0939.

(SDSS J1251-021), two systems have *two* dominant lens galaxies inside the lensed images (SDSS J1618+439 and SDSS J1718+644) and one system has a nearby perturbing companion that also contributes significantly to the light inside the SDSS spectral fiber (SDSS J1205+492). The latter makes its stellar dispersion measurement unreliable. All fifteen remaining systems (see Table 1) are genuine massive early-type lens galaxies, with a redshift range of  $z = 0.06 - 0.33$  and an average stellar velocity dispersion of  $\langle \sigma_{\text{ap}} \rangle = 263 \pm 11 \text{ km s}^{-1}$  (rms of  $44 \text{ km s}^{-1}$ ) inside the SDSS spectroscopic aperture. All conclusions in this paper are based on this sample of 15 galaxies, except for those presented in § 4 and § 5.

## 2.2. The SIE Mass Model

The purposes of the lens models are three-fold: (i) Confirm that the systems are genuine gravitational lenses and that they can be explained through a simple strong lens model, (ii) accurately determine the mass enclosed by the

$\sim 4$  Einstein radii from each other (Kochanek & Apostolakis 1988). Hence, “isolated” implies non-interacting and lensing that is dominated by a single massive galaxy inside the SDSS fibre and several Einstein radii. This constraint is rather weak, affecting only  $\sim 10\%$  of the systems.

lensed images, and (iii) quantify the alignment between the stellar and total mass distribution.

To determine the mass enclosed by the lensed images, we follow the procedure described previously in e.g. Koopmans & Treu (2003) and Treu & Koopmans (2002, 2004). First, we determine the “best-fit” elliptical lens mass model and for that, derive the mass ( $M_{\text{Einst}}$ ) enclosed by the outer (tangential) critical curve. Second, we determine the associated circularly-symmetric mass model – having the same radial density profile – that encloses the same mass inside its critical curve at radius  $R_{\text{Einst}}$ , which we call the Einstein radius.

We use the parametric *Singular Isothermal Ellipsoid* mass model (SIE; Kormann et al. 1994) to describe the projected mass distribution (i.e. convergence) of the lens galaxies (appropriately translated and rotated):

$$\kappa(x, y) = \frac{b_{\text{SIE}} \sqrt{q_{\text{SIE}}}}{2 \sqrt{q_{\text{SIE}}^2 x^2 + y^2}}, \quad (1)$$

with  $q_{\text{SIE}} = (b/a)_{\kappa}$  being the axial ratio of constant elliptical surface density contours. Note that the mass enclosed by the elliptical critical curves, using the above normalization, is independent of  $q_{\text{SIE}}$  (Kormann et al. 1994). The definition of the enclosed mass ( $M_{\text{Einst}}$ )

and the Einstein radius ( $R_{\text{Einst}}$ ) then correspond to those for a classical Singular Isothermal Sphere (SIS with  $q=1$ ; e.g. Binney & Tremaine 1987) and can be associated with a velocity dispersion through  $b_{\text{SIE}} = 4\pi(\sigma_{\text{SIE}}/c)^2 D_d D_{\text{ds}}/D_s$  (see Schneider et al. 1992). This velocity dispersion should *not* be confused with that of the stellar component embedded in an overall isothermal (i.e.  $\rho_{\text{tot}} \propto r^{-2}$ ) mass distribution (e.g. Kochanek 1994). The two quantities can differ, depending on the precise distribution of the stars, their orbital structure inside the overall potential, and the aperture within which the dispersion is measured (Koopmans 2004).

### 2.3. Non-Parametric Source & Image Reconstructions

The complexity of many of the extended lensed images (Paper I) prohibits a simple parameterized description of the source (e.g. point images). Their brightness distributions are therefore reconstructed on a grid of typically  $30 \times 30$  square pixels, with a pixel-size that depends on scale of the lensed images and their magnification (typically between  $0''.01 - 0''.05$ ). We use the regularized non-parametric source reconstruction code described in TK04 and Koopmans (2005) – based on the non-parametric source reconstruction method by Warren & Dye (2003) – with the parametric SIE mass model for the lens potential. We emphasize that the choice of isothermal lens models influences the mass determination within the critical line at a level of a few percent at the most (e.g. Kochanek 1991). This systematic uncertainty is at present negligible in our analyses of the logarithmic density slope (see § 3.4 for a proper discussion), and to first order our lensing and stellar-dynamical analyses can be regarded as independent.

We center the mass model on the brightness peak of the lens galaxy<sup>9</sup> and vary the three remaining model parameters (i.e. lens strength  $b_{\text{SIE}}$ , ellipticity  $q_{\text{SIE}}$  and position angle  $\theta_{\text{SIE}}$ ). At each optimization step, we determine the source structure that minimizes the value of the penalty function  $P = \chi^2 + \lambda R$ , which includes a  $\chi^2$  and a regularization term. The mass-model parameters and  $\lambda$  are varied until  $\chi^2/\text{d.o.f.}$  minimizes to  $\approx 1$  (see Warren & Dye 2003 or Koopmans 2005 for details).

Because the main objective in this paper is to obtain the mass of the galaxy enclosed by its Einstein radius – for subsequent dynamical analyses (§3) – neither the precise choice of the source pixel scale nor the regularization level (i.e. the value of  $\lambda$ ) is found to have a significant impact on the resulting values of  $R_E$  and  $M_{\text{Einst}}$ . We therefore postpone a precise analysis of the structure of the sources to a future publication. The SIE models are sufficiently accurate to (i) confirm the lensed nature of each system, (ii) measure the mass enclosed by the lensed images to a few percent accuracy (see above discussion), and (iii) determine the orientation of the mass distribution with respect to its stellar distribution.

Figure 1 shows the observed structure of the lensed images in the F814W band – after lens galaxy subtraction (Paper I) – and the currently best lensed-image recon-

<sup>9</sup> In several test-cases we find that the mass centroid agrees with the brightness peak to within a pixel. Because the precise position of the mass centroid has negligible effect on the inferred mass enclosed by the lensed images – or the other lens properties – we choose to fix the mass centroid position in order to speed up the convergence process.

struction for each of the fifteen selected lens systems. None of the models require significant external shear above a few percent to improve the models. Therefore we can assume it to be zero for simplicity (see § 2.4.1 for more discussion).

Table 1 summarizes the best-fit parameters from the SIE mass modeling. We find the ratios  $\langle R_{\text{Einst}}/R_{\text{ap}} \rangle = 0.87 \pm 0.05$  (rms of 0.19) between the Einstein radius and the SDSS fiber radius of  $1''.5$ , and  $\langle R_{\text{Einst}}/R_e \rangle = 0.52 \pm 0.04$  (rms of 0.17) between the Einstein radius and the effective radius (see Paper II), with  $\langle R_{\text{Einst}} \rangle = 4.2 \pm 0.4$  kpc (rms of 1.6 kpc). Hence, when discussing the “inner regions” of early-type galaxies, we assume this to be approximately the inner 4 kpc.

### 2.4. Stellar versus Total Mass

Using the SIE mass models, we can assess how well light (i.e. stellar mass) traces the total mass density. In hindsight, this correlation is not surprising, because most of the mass inside  $R_{\text{Einst}}$  is in fact stellar (see § 3.5). However, a significant misalignment or difference in ellipticity between the stellar and dark-matter mass components – even *outside* the Einstein radius – would affect the lens models and show up as differences or increased scatter in the position-angle difference and ellipticity ratio between stellar and total mass. Note also that we implicitly assume an isothermal density profile – which will be further supported in § 3.2 – which in principle could affect the determination of the mass ellipticity and position angle.

#### 2.4.1. Position-Angle Alignment

One test of the lens mass models is the position-angle alignment  $\Delta\theta = (\theta_* - \theta_{\text{SIE}})$  between the stellar component and the SIE lens model. The result is shown in Fig. 2. The average difference is  $\langle \Delta\theta \rangle = 0 \pm 3$  degrees, with an rms spread of 10 degrees. No significant correlation is found between  $\Delta\theta$  and other lens properties. One notices an increase in the rms of  $\Delta\theta$  with increasing  $q_{\text{SIE}}$ , because it becomes increasingly more difficult to determine both  $\theta_*$  and  $\theta_{\text{SIE}}$  for  $q_{\text{SIE}} \rightarrow 1$ : the rms for  $q_{\text{SIE}} < 0.75$  is 3 degrees, whereas it increases to 13 degrees for  $q_{\text{SIE}} > 0.75$ . However, no significant deviations of  $\langle \Delta\theta \rangle$  from zero are found in either bin.

Assuming that (Keeton, Kochanek & Seljak 1997)

$$\langle \Delta\theta^2 \rangle^{1/2} \approx \left\langle \left( \frac{\sin(2[\theta_{\text{SIE}} - \theta_\gamma])}{(\epsilon/3\gamma_{\text{ext}}) \cos(2[\theta_{\text{SIE}} - \theta_\gamma])} \right)^2 \right\rangle^{1/2}, \quad (2)$$

where  $\gamma_{\text{ext}}$  is the external shear,  $\theta_\gamma$  the shear angle, and  $\epsilon = (1 - q_{\text{SIE}}^2)/(1 + q_{\text{SIE}}^2) \approx 0.24$  (see § 2.4.2) and that no correlation between galaxy and external shear orientations exists, we then find that the rms of 10 degrees in  $\Delta\theta$  implies that the average shear has an upper limit  $\langle \gamma_{\text{ext}} \rangle \lesssim 0.035$ . Hence, the alignment between the mass and light position angle confirms that external shear is very small and can be neglected, and that the galaxies are effectively isolated in terms of their gravitational lens properties in the inner  $\sim 4$  kpc. (Note that this does not imply that galaxies are isolated, only that the effect of the field on their lensing properties is small.)

#### 2.4.2. Ellipticity

A second test is to see how well the elliptical isophotal and isodensity contours trace each other. Fig. 2 also shows the ratio between the ellipticity of the stellar light (Paper II;  $q_* = (b/a)_*$ ) and that of the lens mass model ( $q_{\text{SIE}}$ ), as a function of velocity dispersion (i.e. approximately mass). Above  $\sigma_{\text{SIE}}$  of  $\sim 225 \text{ km s}^{-1}$ , the ratio  $\langle q_{\text{SIE}}/q_* \rangle = 0.99$  with an rms of 0.11, hence light traces mass also in ellipticity. Below  $\sim 225 \text{ km s}^{-1}$ , the correlation shows a sudden upturn to  $q_{\text{SIE}}/q_* \sim 1.6$ , which we attribute to the fact that those three galaxies (i.e. J0959+042, J1330-018 and J1420+603) show inclined disk structure and can be classified as lenticular (S0) galaxies (see Paper I). These results strongly suggest that the SIE mass model (further supported in §3) quantifies the mass ellipticity to  $\sim 10\%$  accuracy. We can therefore take the average of  $q_{\text{SIE}}$  as a good measure of the projected isodensity ellipticity of early-type galaxies:  $\langle q_{\text{SIE}} \rangle = 0.78$  with an rms of 0.12. We note that this ellipticity is that of the stellar plus dark-matter mass distribution, not that of the dark-matter halo only. Using

$$\langle q_{\text{SIE}} \rangle = \langle [q_3^2 \cos^2(i) + \sin^2(i)]^{1/2} \rangle, \quad (3)$$

assuming that mass is stratified on oblate constant density ellipsoids and lens-galaxies are randomly oriented (i.e.  $P(i) \propto \sin(i)$ ), this implies an axis ratio in density of  $\langle q_3 \rangle = (c/a)_\rho = 0.66$  with an error of about 0.2.

As an additional check, we assess whether the ellipticity distributions of the SLACS E/S0 lens-galaxy sample and early-type galaxies could possibly be different, which would suggest a possible selection bias. For the 15 SLACS E/S0 lens galaxies, we find  $\langle q_* \rangle = 0.74$  with an rms of 0.13, in excellent agreement with nearby E/S0 galaxies (e.g. Lambas et al. 1992; Odewahn et al. 1997) which peak between 0.7–0.8. We conclude also that the ellipticities of SLACS lens galaxies are similar to those of nearby early-type galaxies.

#### 2.4.3. Does Light follow Mass?

We conclude: (i) The small position-angle difference between the stellar and total mass implies that dark matter is aligned with the stellar component on scales  $\lesssim 4 \text{ kpc}$  and probably also beyond. Even though stellar mass dominates in this region (see § 3.5), a misalignment of stellar and dark matter, even beyond the Einstein radius, can cause an apparent “external” shear (Keeton, Kochanek & Seljak 1997), which is not observed in our sample. (ii) Significant external shear due to nearby galaxies or a misalignment of the outer dark-matter halo with the inner stellar-dominated region is not required in any of the lens model. Significant external shear would in general cause a spread in  $\Delta\theta$  if not accounted for in the models. (iii) The isophotal and isodensity contours of massive elliptical galaxies ( $\gtrsim 225 \text{ km s}^{-1}$ ) seem to follow each other well in their inner regions, whereas the lower velocity dispersion lenticular galaxies have a much rounder mass than light distribution.

#### 2.4.4. The surface brightness bias of SLACS lenses

In Papers I & II, we discussed a bias in favor of more concentrated light-distributions for lens galaxies compared to their parent population with equivalent  $\sigma_{\text{ap}}$ . Because the S/N limit imposed on the velocity-dispersion measurements of lens-galaxy candidates was also imposed on the parent sample, and their distribution in

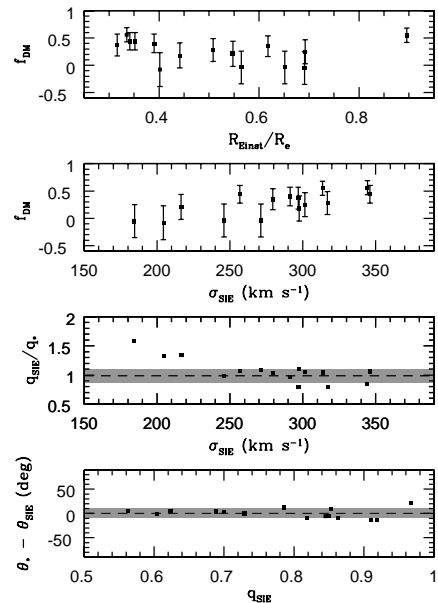


FIG. 2.— (Upper two panels) Inferred dark-matter mass fraction inside the Einstein radius, assuming a constant stellar  $M/L_B$ -ratio as function of E/S0 velocity dispersion (see text). (Third panel) Ratio between the ellipticity (i.e.  $q_* = (b/a)_*$ ) measured from the stellar light (Paper II) and that determined from the SIE mass model ( $q_{\text{SIE}}$ ). Note the tight scatter around unity above  $\sim 225 \text{ km s}^{-1}$  and then the upturn in  $q_{\text{SIE}}/q_*$ , resulting from more disk S0 systems. (Lower Panel) Difference between the position angle measured from the stellar light ( $\theta_*$ ; Paper II) and that determined from the SIE mass model ( $\theta_{\text{SIE}}$ ). Note the increase in rms dispersion with increasing  $q_{\text{SIE}} = (b/a)_\Sigma$ . The rms spread for  $q_{\text{SIE}} < 0.75$  is only 3 degrees, whereas for  $q_{\text{SIE}} > 0.75$  it increases to 13 degrees.

S/N can not be distinguished according to a K-S test, we concluded in Paper II that a bias in S/N due to the finite fiber size is not the underlying cause.

Here we propose another bias that might cause part of this effect. The bias arises because the parent population is chosen to have the same value of  $\sigma_{\text{ap}}$  as that of the lens galaxy, but not necessarily the same mass, i.e. lens cross-section. Suppose we have two galaxies with identical isothermal density profiles and identical velocity dispersions,  $\sigma_{\text{ap}}$ , inside the fiber aperture, but different masses (with  $M_1 < M_2$ ). Because the first galaxy is less massive, the stellar component must be more extended to maintain a similar velocity dispersion inside the aperture. We find that for the range  $R_e/R_{\text{ap}} \approx 0.8 - 3.2$  (see Table 1) the decrease in mass, and therefore lens cross-section, is about 5% for a fixed  $\sigma_{\text{ap}}$ . Whether this bias can partly explain the observed bias, or whether other mechanisms are also important, is not clear and we leave a full analysis to a future paper.

### 3. JOINT LENSING & DYNAMICAL ANALYSIS

In this section, we combine the projected 2D mass-measurement ( $M_E$ ; see § 2) with the stellar velocity dispersion measurement from SDSS spectroscopy ( $\sigma_{\text{ap}}$ ) and the surface brightness distribution from the HST images (see Papers I & II), to determine the 3D logarithmic density slope inside the Einstein radius of each galaxy.



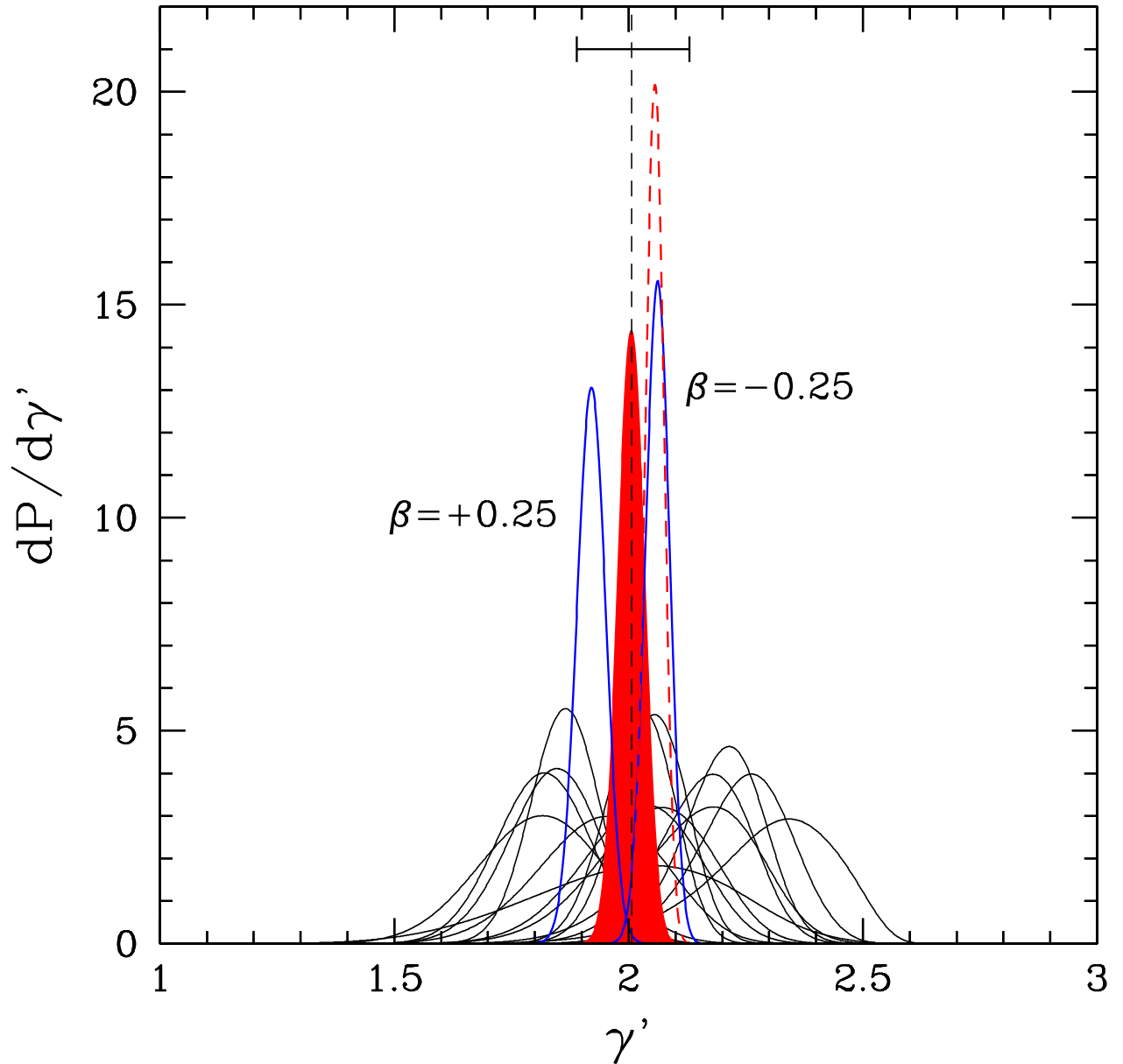


FIG. 3.— Posterior probability distribution functions of the logarithmic total density slope ( $\gamma'$ ; see text). The shaded region (red) indicates the joint probability for  $\gamma'$ , assuming isotropic stellar orbits and a Hernquist (1990) luminosity density profile. The thin solid curves refer to the 15 individual lens systems. The dashed (red) curve assumes a Jaffe (1983) luminosity density profile, leading to a several percent increase in the maximum-likelihood value of  $\gamma'$ . The two solid (blue) curves, indicated by  $\beta = \pm 0.25$ , show the probability functions for radially and tangentially anisotropic stellar orbits respectively (assuming a Hernquist profile for the stellar component). The horizontal bar indicates the  $1\sigma$  intrinsic spread in  $\gamma'$ , corrected for the spread due to measurement errors on the stellar velocity dispersions.

### 3.1. Spherical Jeans Modeling

We model each early-type galaxy as a spherical system, previously discussed in Koopmans & Treu (2003) and Treu & Koopmans (2002, 2004). The modeling is done according to a number of steps and assumptions:

- The stellar plus dark-matter mass distribution of each of the lens galaxies is modeled as

$$\rho_{\text{tot}}(r) = \rho_0 (r/r_0)^{-\gamma'}, \quad (4)$$

where  $\rho_0$  can be uniquely determined from the projected mass  $M(\leq R_{\text{Einst}}) \equiv M_{\text{Einst}}$  and  $r_0$  can be set arbitrarily. In §3.5 we discuss in more detail why we make this assumption for the family of total-density profiles. The only remaining free parameter in the density distribution is therefore the logarithmic density slope  $\gamma'$  [Note that  $\gamma' = -d \log(\rho_{\text{tot}})/d \log(r)$ ]. As discussed in TK04, the results are very insensitive to a cutoff at large radii (i.e. beyond several effective radii) in the dynamical

analysis.

- The stellar component is treated as a massless tracer (i.e.  $M_*/L \rightarrow 0$ ) in the gravitational potential of the total density profile. We assume a stellar density

$$\rho_*(r) = \frac{(3 - \gamma_*)M_*r_*}{4\pi r^{\gamma_*}(r + r_*)^{(4-\gamma_*)}}, \quad (5)$$

where  $M_* = L_B \times (M_*/L_B)$  is the total stellar mass (assumed to be zero in the limit),  $r_*$  is a break-radius and  $\gamma_*$  in the inner logarithmic stellar-density slope. For the Hernquist (1990) profile  $\gamma_* = 1$  and  $r_* = R_e/1.8153$ , such that half of the projected light is inside  $R_e$ . The projected Hernquist profile closely resembles an  $R^{1/4}$  profile with which we determined the effective radii of each lens galaxy (see Paper II). In case of the Jaffe (1983) profile,  $\gamma_* = 2$  and  $r_* = R_e/0.7447$ . The two profiles delineate a range of possible models, bracketing the observed range of galaxy profiles, useful to test for potential systematics.

- Given the total density (i.e. gravitational potential) and the luminosity density, we solve the spherical Jeans equations (see Binney & Tremaine 1987), to determine the line-of-sight stellar velocity dispersion as function of radius. The calculations are done assuming different (constant) values for the velocity anisotropy of the stellar orbits (see e.g. Gerhard et al. 2001) with  $\beta \equiv 1 - \langle v_\theta^2 \rangle / \langle v_r^2 \rangle$ . Tangential anisotropy has  $\beta < 0$ , whereas radial anisotropy has  $\beta > 0$ .
- Both seeing and aperture effects are accounted for in the dynamical models. The observed stellar velocity dispersion is a luminosity-weighted average dispersion inside the SDSS fiber aperture. We assume Gaussian seeing with  $\langle \text{FWHM} \rangle = 1.5$  arcsec for the SDSS spectroscopic observations, although the exact value is almost irrelevant, given the three-arcsec diameter spectroscopic fiber aperture.
- The probability density of  $\gamma'$  is then given by

$$\frac{dP}{d\gamma'} \propto e^{-\chi^2/2}, \quad (6)$$

with  $\chi^2 = [(\sigma_{\text{ap}} - \sigma_{\text{mod}})/\delta\sigma_a]^2$  and  $\delta\sigma_{\text{ap}}$  is the  $1\sigma$  error on the aperture velocity dispersion measured from the SDSS spectra. The integrated probability density function is normalized to unity.

### 3.2. The Logarithmic Density Slope

Following the procedure described in §3.1, we determine the probability density functions for  $\gamma'$  for each of the fifteen early-type galaxies, assuming a Hernquist luminosity density profile with  $\beta = 0$ . The results are shown in Fig. 3 (thin black solid curves) and summarized in Table 1.

Also shown is the joint probability (red shaded area),  $P_{\text{joint}} \propto \prod_i (dP_i/d\gamma')$ , from which we determine an average logarithmic density slope of

$$\langle \gamma' \rangle = 2.01_{-0.03}^{+0.02} \quad (68\% \text{ C.L.})$$

for the ensemble of galaxies. The fractional spread in  $\gamma'$  of  $\sim 10\%$  is partly due to the measurement error  $\delta\sigma_{\text{ap}}$ . To determine the true intrinsic spread around  $\langle \gamma' \rangle$  in the ensemble of systems, we approximate the likelihood function of  $\gamma'_i$  for each system by a Gaussian with a  $1\sigma$  error of  $\delta\gamma'_i$ . Second, we assume that the slope  $\gamma'_i$  of each system is drawn from a underlying Gaussian distribution around  $\langle \gamma' \rangle$  with an intrinsic  $1\sigma$  spread of  $\sigma_{\gamma'}$ .

The maximum-likelihood solution for  $\sigma_{\gamma'}$  (ignoring the much smaller error on  $\langle \gamma' \rangle$ ) is then found from:

$$\sum_i \left[ \frac{(\gamma'_i - \langle \gamma' \rangle)^2 - \sigma_{\gamma'}^2 - \delta\gamma'_i{}^2}{(\sigma_{\gamma'}^2 + \delta\gamma'_i{}^2)} \right] = 0. \quad (7)$$

The solution of this equation is  $\sigma_{\gamma'} = 0.12$  for the sample of fifteen early-type galaxies. This is a very small *intrinsic* spread of only 6% around the average value, considering that many effects have not yet been accounted for.

#### 3.2.1. Implications for $H_0$ from lensing

We comment that the small intrinsic scatter in  $\gamma'$  of around 6% suggests that these low-redshift ( $z \lesssim 0.3$ ) massive early-type galaxies could be ideal for measuring  $H_0$  from time-delays<sup>10</sup>, with an expected rms scatter of around 12% between systems if they are assumed to be perfectly isothermal (TK04). At higher redshifts – where both external shear and convergence from the group and/or large-scale-structure environment of the lens galaxies become more important – the same assumption can lead to a larger (i.e. around 30%) systematic scatter in  $H_0$  (see TK04 for a full discussion). We note also that we measure the average density slope *inside*  $R_{\text{Einst}}$ , whereas the time-delay depends on the local density slope *inside the annulus* between the lensed images (Kochanek 2002), which could have a different value and most likely a larger scatter (because it is not averaged).

#### 3.3. Random Errors on the Density Slope

The assumption of an isothermal lens mass model (see §2.1) systematically affects the mass determination of the lens galaxy inside its Einstein radius at most at the few-percent level (see Kochanek 1991 and §3.4). In addition, the mass determination has a random error, which we expect to be very small because of the high S/N-ratio data that we use to fit the models<sup>11</sup>. The alignment of mass and light (§2.4) also suggests that the remaining degeneracies in the mass model are too small to lead to a biased mass estimate [on average].

In the rest of this section we show that residual errors on the lensing-based mass determination within the critical line are negligible with respect to the measurement errors on the stellar velocity dispersion. In the spherically

<sup>10</sup> Note that this requires a variable source. In case of an active galactic nucleus source, however, the lensed images often outshine the lens galaxy, making a joint lensing and dynamical analysis more difficult. However, SNe in star-forming lensed sources could provide very accurate time-delays (Holz 2001; Bolton & Burles 2003; Moustakas et al. in prep.).

<sup>11</sup> The fractional random error on the mass is  $\delta M_{\text{Einst}} \approx 2 \cdot \delta\Delta\theta$  for the SIE mass model. Because the error on the image separation  $\Delta\theta \approx 2b_{\text{SIE}}$  is typically the width of the lensed arcs divided by twice the S/N-ratio, we expect the random error on  $M_{\text{Einst}}$  to be less than a few percent. In the low-S/N case of SDSS J1402+634 (Bolton et al. 2005), for example, we found a random error of  $\sim 3\%$ . We expect the other SLACS systems to have much smaller errors because of their typically much higher S/N-ratio images.

symmetric case with power-law dependencies for the luminosity density and total density, one can show (Koopmans 2004) that the fractional error  $\delta_{\gamma'} \equiv \delta\gamma'/\gamma' \ll 1$  is related to those on the mass ( $M_{\text{Einst}}$ ) and the measured stellar velocity dispersion ( $\sigma_{\text{ap}}$ ) by

$$\begin{aligned} \delta_{\sigma(\leq R_{\text{ap}})} &= \frac{1}{2}\delta_{M_{\text{Einst}}} + \frac{1}{2}\left(\frac{\partial \log f}{\partial \log \gamma'} - \gamma' \log \left[\frac{R_{\text{ap}}}{R_{\text{Einst}}}\right]\right) \cdot \delta_{\gamma'} \\ &\equiv \frac{1}{2}(\delta_{M_{\text{Einst}}} + \alpha_g \cdot \delta_{\gamma'}), \end{aligned} \quad (8)$$

from which one finds (assuming independent errors)

$$\langle \delta_{\gamma'}^2 \rangle = \alpha_g^{-2} \{ \langle \delta_{M_{\text{Einst}}}^2 \rangle + 4 \langle \delta_{\sigma}^2 \rangle \}. \quad (9)$$

Here  $\alpha_g$  is typically of order a few and the function  $f$  depends on the logarithmic slopes of the total and luminosity density profiles and  $\beta$  (see Koopmans 2004 for its full expression in terms of gamma-functions). The pre-factor of four and the typical fractional errors on  $\delta_{\sigma} \sim 0.05$  from SDSS spectroscopy (see Table 1), implies that  $\delta_{M_{\text{Einst}}}$  can be neglected given the current kinematic data quality. The fractional error on the logarithmic density slope is therefore, to first order, equal to the fractional error on the measured stellar velocity dispersion. Even though the Hernquist and Jaffe luminosity density functions follow a broken power-law (§3.1), this relation holds in our joint lensing and dynamical analysis with a fractional spread in density slopes  $\gamma'$  very close to that in stellar velocity dispersions (c.f. Paper II and TK04).

### 3.4. Systematic Uncertainties on the Density Slope

The dominant systematic uncertainties in the current analysis are probably the unknown stellar velocity anisotropy, the assumption of spherical symmetry in the dynamical models, deviations of the inner luminosity density profile from the assumed Hernquist luminosity density profile and the possible contribution to the mass inside the Einstein radius by the surrounding field galaxies.

To assess some of these uncertainties, we redo our analysis for a change of anisotropy parameters  $\Delta\beta = [-0.25, +0.25]$  (with a Hernquist profile). The resulting change in the average value of  $\gamma'$  is relatively small  $\Delta\gamma' = [+0.05, -0.09]$ . Similarly, if we assume a Jaffe (1983) luminosity density profile, we find  $\Delta\gamma' = +0.05$  (assuming  $\beta = 0$ ).

Because of their comparable scales, the small value of  $\sigma_{\gamma'}$  could partly be due to some remaining systematic effects. We note that the ensemble could also be more radially anisotropic (e.g. Gerhard et al. 2001) and/or have a luminosity density cusp steeper than Hernquist, but the above analysis shows these systematic shifts in  $\gamma'$  to be  $\lesssim 5\%$  for reasonable assumptions. We note also that the small intrinsic spread in  $\gamma'$ , in principle, allows us to set an upper limit on the average anisotropy of their velocity ellipsoid, using the tensor virial theorem (Binney 1978; Sandy Faber and Chris Kochanek, private communications). This could potentially lead to a correlation between the stellar mass ellipticity and its velocity dispersion and therefore with the inferred density slope. To test this, we plot  $\gamma'$  against  $q_*$  in Fig.5: no significant correction is found and the effect must therefore be small. We defer a more thorough analysis to a future publication, that will make additional use of more

detailed kinematic data obtained from IFS observations of several of the SLACS lens galaxies and two-integral dynamical models.

If the field around the lens galaxies contributes significantly to the enclosed mass (i.e. to the convergence inside the Einstein radius), it biases  $\gamma'$  to lower values, if not accounted for (see e.g. TK04 for a discussion). There are several reasons why we believe this contribution to be relative small for the SLACS lens systems. First, we found that each system can be modeled as a SIE without requiring significant external shear. In general the strength of the shear equals roughly the convergence of the field (if dominated by only a few systems). Second, because SLACS lens systems are at relatively low redshifts compared to lens systems known to date (typically at  $z_l \sim 0.6$ ), the angular distance between the lens galaxies and their nearest neighbors (in units of the Einstein radius) is larger than at higher redshift. Consequently, the influence of the field on the lens system is lower by at least a factor of a few compared to high- $z$  systems (e.g. Paper II). In addition, because the external convergence  $\kappa_{\text{ext}}$  lowers the mass fractionally by  $\sim \delta_{M_{\text{Einst}}}$ , we find from Equation 9 that  $\delta_{\gamma'} \sim \kappa_{\text{ext}}/\alpha_g$ . Hence, even a high external shear or convergence of 0.1 – easily detectable by the lens models – would affect  $\gamma'$  at most at the  $\sim 5\%$  level (for typical  $\alpha_g \sim 2$ ). On average, however, the expected external convergence is only a few percent (e.g. Fassnacht & Lubin 2002; Keeton & Zabludoff 2004; Dalal & Watson 2004), reducing its influence to less than a few percent.

Another systematic uncertainty could stem from the determination of  $\sigma_{\text{ap}}$  from the SDSS spectrum. If SDSS velocity dispersions were systematically biased, this would skew  $\gamma'$  in one or the other direction, although there is no reason to assume this bias exists. Moreover, Bernardi et al. (2003) estimate systematic uncertainties on the measured velocity dispersions of  $<3\%$ . The ongoing IFS observations, discussed above, will allow us to rigorously test this.

#### 3.4.1. The assumption of a power-law density profile

Finally, the most serious assumption is the shape of the density-profile itself (§3.1), i.e. a power-law. This assumption can be tested, however. If either the density profiles of lens galaxies are different from a power-law, but have the same shape for each galaxy (scaled to a common scale), or, if they are different from a power-law and different between lens galaxies, in both cases one expects the inferred (average) logarithmic density slope inside  $R_{\text{Einst}}$  to change with the ratio ( $R_{\text{Einst}}/R_e$ ). For example, if the profile is a broken power-law with a change in slope inside  $R_{\text{Einst}}$ , one expects  $\gamma'$  to change depending on where the change in slope occurs with respect to the effective radius. One would find some ‘‘average’’ slope weighed by luminosity and kinematic profile, and expect this to change as function of ( $R_{\text{Einst}}/R_e$ ), because  $R_{\text{Einst}}$  depends mostly on the relative distances of the lens and the source and is not a physical scale of the lens galaxy itself. The absence of any clear systematic correlation between  $\gamma'$  and this ratio (see Fig.5), however, shows that this is not the case. The small deviations of  $\gamma'$  from 2.0 further support this (§3.2). We conclude that the assumption of a single power-law shape for the total density profile is valid at the level warranted by the

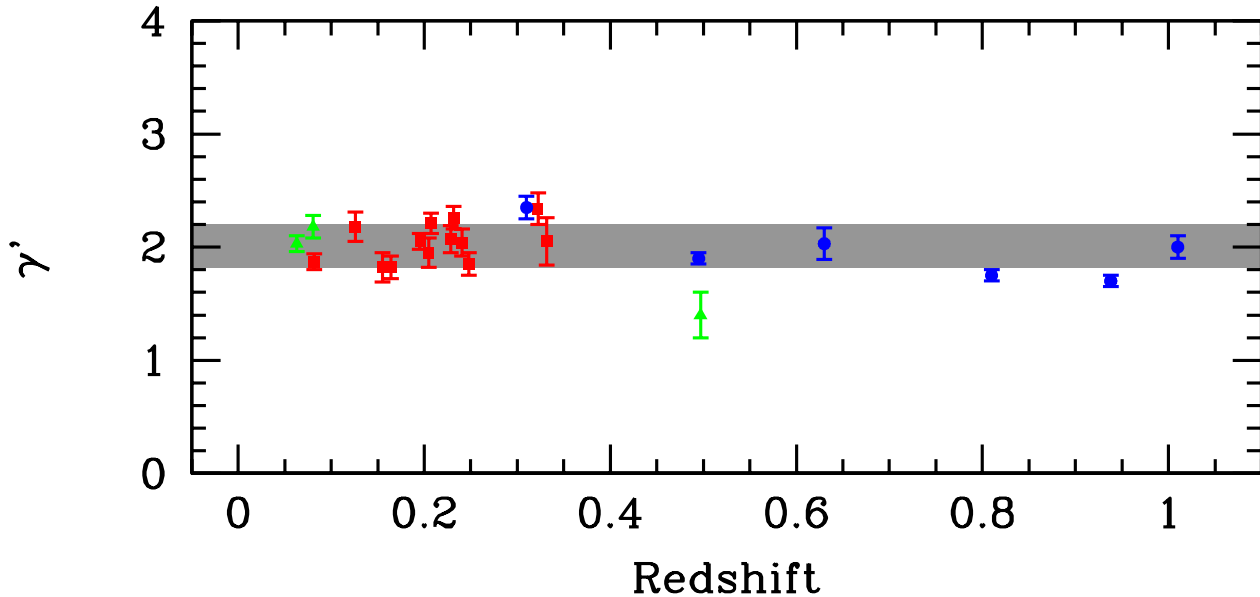


FIG. 4.— The logarithmic density slopes ( $\gamma' = -d \log \rho_{\text{tot}} / d \log r$ ) of field early-type lens galaxies, plotted against redshift. The (grey) box indicates the rms spread (0.19; partly due to measurement errors) around the straight average of all SLACS/LSD systems with  $\sigma_{\text{ap}} \geq 200 \text{ km s}^{-1}$  (2.01; the same as from the complete SLACS sample). The red solid squares are from the SLACS Survey, and the blue solid circles from the LSD Survey plus two additional systems (see text). The green solid triangles are SLACS/LSD systems with  $\sigma_{\text{ap}} < 200 \text{ km s}^{-1}$ .

current data.

### 3.5. Dark Matter Inside the Einstein Radius

The spatially resolved kinematic profile and the high-quality data of *HST* allowed TK04 to do separate analyses of the luminous and dark matter in individual early-type lens galaxies. The larger SDSS fiber aperture, the absence of spatially resolved information, and the higher stellar mass fraction inside  $R_{\text{Einst}}$  prevent us from performing a similarly precise analysis. This will require higher spatial resolution kinematic data (e.g. with integral-field spectroscopy) and is left for future work.

Despite this limitation, we can still infer an average dark-matter mass fraction inside the Einstein radii of the ensemble of systems, keeping some caveats in mind (see discussion below). To do this, we first solve the spherical Jeans equation for two-component mass models, assuming a Hernquist luminosity density profile scaled by a stellar mass-to-light ratio, plus a dark-matter density component with density profile  $\rho_{\text{DM}} \propto r^{-\gamma}$ , and assuming that  $\beta = 0$  (see Koopmans & Treu 2003 and Treu & Koopmans 2002, 2004 for more details). The sum of both mass components must be  $M_{\text{Einst}}$  inside the Einstein radius. This leads to a likelihood grid as function of stellar  $M_*/L_B$  and dark-matter density slope  $\gamma$  (see e.g. TK04). Second, a Gaussian prior is set on the value of  $M_*/L_B$ , assuming an average local restframe B-band stellar mass-to-light ratio of  $7.3 M_{\odot}/L_{\odot,B}$  with a  $1-\sigma$  of  $2.1 M_{\odot}/L_{\odot,B}$  (e.g. Gerhard et al. 2001; see also TK04) and correcting this for the average passive evolution of  $d \log(M/L_B)/dz = -0.69 \pm 0.08$  found from the sample in Paper II, which brightens galaxies with

increasing redshift. The luminosity corrections are small ( $\lesssim 20\%$ , however, for SLACS galaxies at redshifts below 0.33). Finally, we marginalize the resulting probability distribution (including the mass-to-light ratio prior) over  $\gamma$  to obtain the likelihood function of the dark-matter mass fraction inside  $R_{\text{Einst}}$ :  $f_{\text{DM}} = 1 - f_*$ . The stellar mass fraction  $f_*$  is given by the maximum-likelihood value of  $M_*/L_B$  divided by the maximum allowed value of  $M_*/L_B$ <sup>12</sup>. The results are listed in Table 1. The straight average of  $f_{\text{DM}}$  is found to be  $\langle f_{\text{DM}} \rangle = 0.25 \pm 0.06$  (rms of 0.22) inside  $\langle R_{\text{Einst}} \rangle = 4.2 \pm 0.4 \text{ kpc}$  (rms of 1.6 kpc) with a large range between about 0% to 60%.

We note that none of the stellar mass-to-light ratios significantly exceeds the maximum set by the inequality  $M_*(\leq R_{\text{Einst}}) \leq M_{\text{Einst}}$ , which can be regarded as an additional (although weak) check on the validity of our assumptions. Finally, we investigate whether the dark-matter fraction ( $f_{\text{DM}} = 1 - f_*$ ) inside the Einstein radius correlates with other lens properties. In Fig. 2, we plot  $f_{\text{DM}}$  against  $\sigma_{\text{SIE}}$  and do indeed find a correlation (correlation coefficient  $r = 0.74$ ). This correlation is predominantly due to the low inferred dark-matter mass fraction in the low-mass (i.e. low dispersion) galaxies, whereas the higher mass systems seem to have  $f_{\text{DM}} \approx 0.4 - 0.6$ . This correlation can either be true, i.e. low-mass galaxies have less dark matter in their inner regions (Napolitano et al. 2005), or be a result of the break-down of one of our assumptions.

We think that the latter is the most likely explanation, because the three lowest-mass systems with  $f_{\text{DM}} \approx 0$  (all

<sup>12</sup> The stellar mass must satisfy  $M_*(\leq R_{\text{Einst}}) \leq M_{\text{Einst}}$

S0 galaxies) have values of  $q_{\text{SIE}}/q_* \gg 1$ , suggesting that dark matter contributes significantly to their inner regions similar to spiral galaxies. In fact, the assumption of a constant stellar  $M/L_B$  ratio, independent of  $\sigma_{\text{SIE}}$ , is probably not entirely correct. Within the “downsizing” scenario which leads to a tilt in the Fundamental Plane (see e.g. Paper II), a lower stellar  $M/L_B$  ratio is expected for S0 galaxies. This leads to a lower inferred dark-matter mass fraction inside the Einstein radius. In addition, we find no strong trend of dark-matter mass fraction with the ratio of Einstein radius over effective radius (Fig.2).

We therefore conclude that the inferred values of  $f_{\text{DM}}$  only give a general indication<sup>13</sup>. The other results in this paper, however, do not depend on the stellar  $M/L_B$  assumption. As mentioned above, we are obtaining higher spatial resolution kinematic data to improve upon this without assuming a stellar mass-to-light ratio.

#### 4. THE EVOLUTION OF THE INNER DENSITY PROFILE OF EARLY-TYPE GALAXIES

In combination with results from the Lenses Structure & Dynamics (LSD) survey (Koopmans & Treu 2002, 2003; Treu & Koopmans 2002, 2004) and from two more lens systems for which stellar velocity dispersions are measured and analyzed in a homogenous way (Treu & Koopmans 2002b; Koopmans et al. 2003) at  $z \gtrsim 0.3$ , we are now in a position to measure the evolution in the average logarithmic density slope of early-type galaxies to  $z \approx 1$ , if present. Since these systems have been selected in different ways, we initially limit our analysis to the most massive early-type galaxies with  $\sigma_{\text{ap}} > 200 \text{ km s}^{-1}$  (i.e.  $\gtrsim L_*$ ). Because the brightness profile, stellar velocity dispersion, and lens models are easier to obtain for these systems, we can expect smaller systematic uncertainties in this sample. Only 3 systems do not meet this criterion. This cut also simplifies comparisons to massive galaxies in numerical simulations (e.g. Meza et al. 2003; Kawata & Gibson 2003).

Fig. 4 shows all systems from the SLACS and LSD surveys, including PG1115+080 (Treu & Koopmans 2002) and B1608+656-G1 (Koopmans et al. 2003). The unweighted average value of  $\gamma'$  for the LSD/SLACS systems with  $\sigma_{\text{ap}} > 200 \text{ km s}^{-1}$  is 2.01 (similar to the SLACS sample alone) and an rms of 0.19 is found. To measure the evolution of the density slope, we do an unweighted linear fit<sup>14</sup> to the ensemble of systems, finding  $\langle \gamma' \rangle(z) = (2.10 \pm 0.07) - \alpha_{\gamma'} \cdot z$  with

$$\alpha_{\gamma'} \equiv \frac{d\langle \gamma' \rangle}{dz} = 0.23 \pm 0.16 \quad (1 \sigma)$$

below  $z \lesssim 1$ . This is marginally consistent with *no* evolution, or with a change in  $\langle \gamma' \rangle$  of  $\sim 10\%$  in the last  $\sim 7$  Gyr. If we include those systems with  $\sigma_{\text{ap}} < 200 \text{ km s}^{-1}$  we find  $\alpha_{\gamma'} = 0.29 \pm 0.17$ . More recently, Hamana et al. (2005) analyzed two more systems, B2045+265 (Fassnacht et al. 1999) and HST 14113+5211 (Fisher et al.

<sup>13</sup> Note that the dark-matter mass fraction is not given within a physical radius, such as the effective radius, because it requires a more proper density model for stellar and dark matter which is not possible with the current data.

<sup>14</sup> Because of the relative small ensemble of systems at higher redshifts and their less well-know selection effect, the intrinsic spread in  $\gamma'$  might be poorly sampled. A weighted fit would then bias the result to a few systems.

1998); inclusion of their results gives  $\alpha_{\gamma'} = 0.34 \pm 0.15$ . However, the former lens system has a disputed source redshift and the latter a massive nearby cluster, leading us to not select these systems in the LSD Survey. Despite combining variously-selected lens systems, the results are robust against changes in the cut in  $\sigma_{\text{ap}}$  or the selection of included lens systems.

To our knowledge, this is the first constraint on the evolution of the logarithmic density slope in the inner regions of early-type galaxies to redshifts as high as  $z \approx 1$ , although we note that a progenitor bias could play a role here in that we only select those systems (from the SDSS LRG and MAIN samples) that have not undergone recent major mergers that resulted in star-formation (i.e. large  $\text{EW}_{\text{H}\alpha}$ ; although major dry mergers could still have occurred).

#### 4.1. Other Correlations

To test whether  $\gamma'$  correlates with other quantities of interest, in Fig. 5 we plot  $\gamma'$ , from only the SLACS early-type galaxies, against (i) the Einstein radius (in units of effective radius), (ii) the projected mass inside the effective radius, and (iii) the effective surface brightness. The first allows us to assess whether the density slopes change over the region where dark matter becomes more dominant, the second whether the density slope depends on galaxy mass and the third whether more concentrated stellar distribution imply a more concentrated density distribution (see Papers I & II). We find in all three cases *no* significant correlation. We therefore conclude that *at the current level of significance* the logarithmic density slope appears a constant and only in combination with the LSD systems a marginal trend with redshift might be observed.

### 5. SUMMARY OF RESULTS

The *Sloan Lens ACS* (SLACS) Survey has provided the largest uniformly selected sample of massive early-type lens galaxies to date (Papers I & II). We used a subsample of fifteen early-type lens galaxies with a redshift range of  $z = 0.06 - 0.33$  and an unweighted average stellar velocity dispersion of  $\langle \sigma_{\text{ap}} \rangle = 263 \pm 11 \text{ km s}^{-1}$  for a joint lensing and dynamical analysis, finding the following results:

- The average logarithmic density slope of the *total* mass density of  $\langle \gamma' \rangle = 2.01_{-0.03}^{+0.02}$  (68% C.L.) assuming a total density profile of  $\rho_{\text{tot}} \propto r^{-\gamma'}$  and no anisotropy (i.e.  $\beta = 0$ ). Systematic uncertainties (e.g. orbital anisotropy and different luminosity density cusps) are expected to be  $\lesssim 5 - 10\%$  [see § 3.2].
- The *intrinsic* spread in the logarithmic density slope is at most 6%, i.e.  $\sigma_{\gamma'} = 0.12$  (the  $1 \sigma$  of the assumed Gaussian spread) [see § 3.2], after accounting for measurement errors.
- The average position-angle difference between the stellar light component and the total mass component is found to be  $\langle \Delta\theta \rangle = 0 \pm 3$  degrees with 10 degrees rms, setting an upper limit of  $\langle \gamma_{\text{ext}} \rangle \lesssim 0.035$  on the average external shear. [see § 2.4].

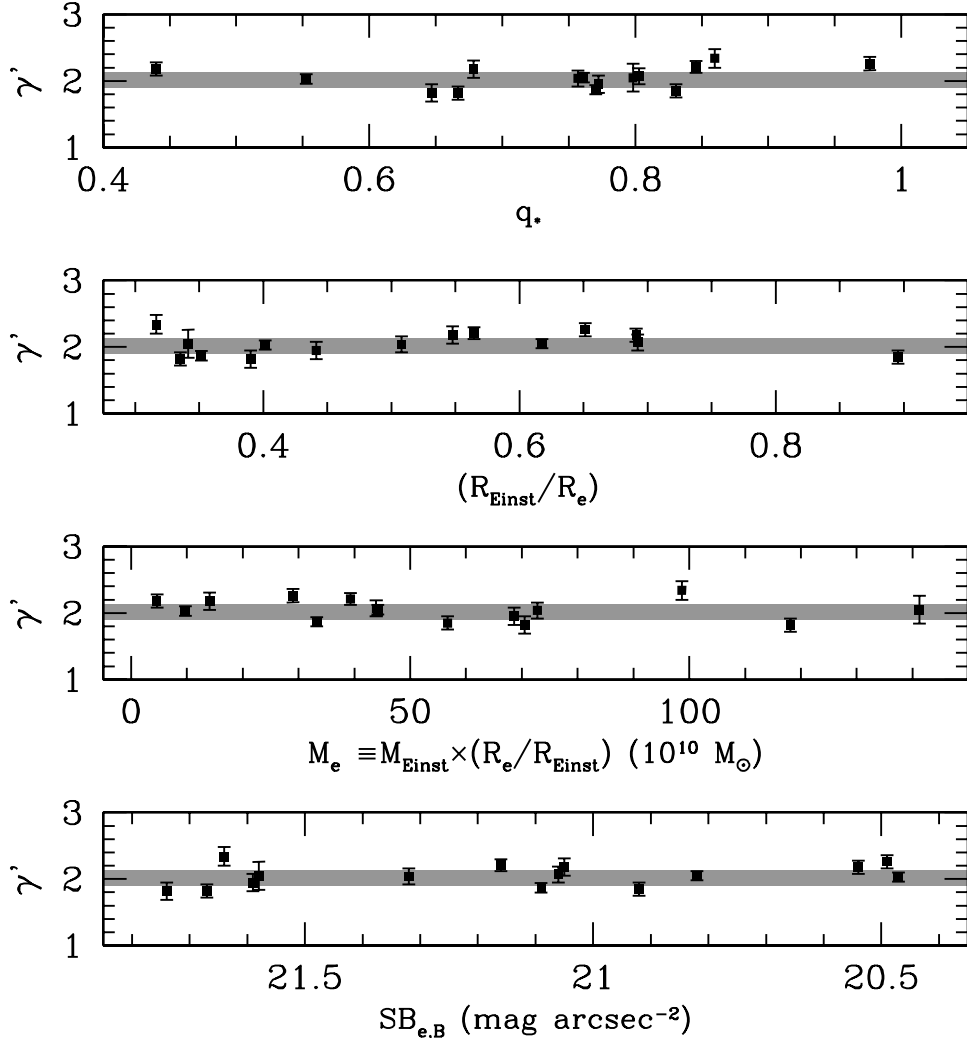


FIG. 5.— The logarithmic density slope of SLACS lens galaxies as function of stellar ellipticity, the (normalized) Einstein radius, the projected mass inside the effective radius and the effective surface brightness, respectively. In none of these cases, a significant correlation is found. In particular, the absence of any correlation between  $\gamma'$  and  $SB_{e,B}$  argues against more condensed early-type galaxies having a steeper density profile. Similarly, the absence of correlation with  $(R_{\text{Einst}}/R_e)$  suggests that in the transition region from a stellar to dark matter dominated density distribution, the logarithmic density slope is unchanged.

- The ellipticity of the total surface-density is  $\langle q_{\text{SIE}} \rangle = 0.78 \pm 0.03$  (rms of 0.12) and  $\langle q_{\text{SIE}}/q_* \rangle = 0.99 \pm 0.03$  (rms of 0.11) for  $\sigma \gtrsim 225 \text{ km s}^{-1}$ . Assuming an oblate mass distribution and random orientations, this implies  $\langle q_3 \rangle \equiv \langle (c/a)_\rho \rangle = 0.7$  with an error of 0.2 [see § 2.4].
- The unweighted average projected dark-matter mass fraction is  $\langle f_{\text{DM}} \rangle = 0.25 \pm 0.06$  (rms of 0.22) inside  $\langle R_{\text{Einst}} \rangle = 4.2 \pm 0.4 \text{ kpc}$  (rms of 1.6 kpc) [see § 3.5].
- The evolution of the total density slope for galaxies with  $\sigma_{\text{ap}} \geq 200 \text{ km s}^{-1}$  ( $> L_*$ ), inside half an effective radius,  $\langle \gamma' \rangle(z) = (2.10 \pm 0.07) - (0.23 \pm 0.16) \cdot z$  for the range  $z = 0.08 - 1.01$  (combined sample from the SLACS and LSD Surveys) [see § 4].

*Summarising: Massive early-type galaxies below  $z \approx 1$  have remarkably homogeneous inner mass density profiles, i.e.  $\rho_{\text{tot}} \propto r^{-2}$  (equivalent to a flat rotation curve for a rotation supported system), and very close alignment between stellar and total mass. There is no evidence for significant evolution in the ensemble average logarithmic density slope of dark plus stellar mass below a redshift of one in their inner half to one effective radius.*

## 6. DISCUSSION & OPEN ISSUES

Although the isothermal nature of early-type galaxies has previously been shown through dynamical, X-ray and lensing studies (see § 1), our results are the first where the logarithmic density-slope of individual early-type galaxies have been determined beyond the local Universe (i.e. between  $z = 0.08$  and  $1.01$ ), based on a well-defined sample of systems from the SLACS Survey (Papers I & II), complemented with the most massive systems from the

LSD Survey (e.g. TK04) at higher redshift. These combined results provide the first direct constraint on the evolution of the inner regions of massive early-type galaxies with cosmic time.

Even though we find no evidence for significant evolution in the inner regions of massive early-type galaxies, this does *not* require that early-type galaxies at  $z \approx 0$  have the same formation or assembly epoch as those studied at  $z \approx 1$ . A similar “progenitor bias” as in FP studies might play a role here as well (e.g. van Dokkum & Franx 2001). This possibility should always be kept in mind in comparing galaxies at different redshifts.

Because the number-density of massive early-type galaxies does not appear to have changed by more than a factor of two since  $z \approx 1$  (e.g. Im et al. 2002; Bell et al. 2004; Treu et al. 2005a&b; Juneau et al. 2005) and no major evolution of  $\gamma'$  has been found in our combined SLACS plus LSD sample (see Fig. 4), one can conclude that either the time-scale for their inner regions to relax to isothermality must be very short (less than a Gyr), if roughly half of the ellipticals in the sample at  $z \lesssim 0.3$  formed at redshifts below one, or that the inner regions of most early-type observed at  $z \lesssim 1$  were already in place at higher redshifts, consistent with collisionless numerical simulations (e.g. Wechsler et al. 2002; Zhao et al. 2003; Gao et al. 2004).

### 6.1. Formation Scenarios

How do these observational results fit into a hierarchical scenario where massive early-type galaxies form through gas-rich or gas-poor (i.e. “dry”) mergers? The SLACS and LSD samples provide three core pieces of information on stellar-population *and* structural properties of early-type galaxies :

1. Their inner regions consist of an old stellar population formed at  $z \gg 1$ , with some evidence for secondary infall at lower redshifts of at most  $\sim 10\%$  in mass (Paper II).
2. Their inner regions have nearly isothermal density profiles and show remarkably little intrinsic spread in their density slopes.
3. Their inner regions show little evolution below  $z \approx 1$  in the ensemble average of the density slope.

With these pieces of information, we can examine the likelihood of different formation scenarios, not only in the context of their stellar populations e.g. through the FP studies (see Paper II), but also based on their structural properties and structural evolution (this paper).

#### 6.1.1. Collisional “Wet” Mergers

It has been suggested that massive elliptical form predominantly at  $z < 1$  from the mergers of gas-rich disk galaxies (e.g. Kauffmann, Charlot & White 1996; Kauffmann & Charlot 1998). Although this scenario might quickly lead to relaxed galaxies – after a rapid star-burst triggered by the gas-shocks and inflows and the subsequent relaxation of the resulting stellar populations in several dynamical time-scales (e.g. Barnes & Hernquist 1991, 1992, 1996; Mihos & Hernquist 1996) – the relatively old stellar populations seems to exclude this scenario as a dominant effect at low redshifts in the SLACS and LSD early-type galaxies (see Paper II).

Similarly, we conclude that no significant “secular evolution” in the form, e.g., of adiabatic contraction (e.g. Blumenthal et al. 1986; Ryden & Gunn 1987; Navarro & Benz 1991; Dubinski 1994; Jesseit, Naab & Burkert 2002; Gnedin et al. 2004; Kazantzidis et al. 2004) of the inner regions ( $\sim 4$  kpc) seems to have occurred at  $z \lesssim 1$  in the inner regions of the population of early-type galaxies that was already in place at  $z \approx 1$ . This would lead to a continuous increase in their ensemble average inner density slope toward lower redshifts. In Treu & Koopmans (2002), we tentatively concluded this already, based on the analysis of a single lens system MG2016+112 at  $z=1.01$ , with an upper limit on its inner dark-matter density slope only marginally consistent with that predicted by numerical simulations (e.g. Navarro et al. 1996; Moore et al. 1998) after adiabatic contraction.

A more gradual infall of gas-rich satellites, leading to secondary episodes of star formation (e.g. Trager et al. 2000; Treu et al. 2002) seems limited on average to  $\sim 10\%$  in mass below redshifts of unity (see also Treu et al. 2005a,b). Such an infall could alter the average structural properties of the population of early-type galaxies; at present, we can not exclude that the (marginally) positive value of  $\alpha_{\gamma'} = 0.23 \pm 0.16$  (see §4) could be due to a slight change of the inner regions of massive ellipticals, as a result of secondary gas-infall. However, it does not appear to be a dominant effect in the structural evolution of most massive early-type galaxies at low redshifts.

Hence, the observational evidence appears to show that most of the massive SLACS and LSD early-type galaxies were already in place at  $z \approx 1$  in terms of their dominant old stellar population *and* dynamically, although very rapid “dry” mergers of several of the lower-redshift galaxies can not be fully excluded.

Beyond redshifts of  $z \approx 1$  and in disk galaxies (which might later assemble into massive elliptical galaxies), gas infall and dissipational processes are most likely very important (e.g. Mo, Mao & White 1998; Abadi et al. 2003a&b). The total density profile of the simulated disk galaxy at  $z \approx 4$  in Gnedin et al. (2004), for example, is close to isothermal in the inner 1–4 kpc, although steeper inside the inner  $\sim 1$  kpc. Hence, even though these simulations suggest that adiabatic contraction plays a role in the formation for disk galaxies at high redshift, it remains unclear how it could lead to such a tight intrinsic scatter of  $\lesssim 6\%$  in the logarithmic density slopes around  $\gamma' = 2$  of early-type galaxies (see §3.2), that presumably form from the mergers of these disk galaxies (e.g. Toomre & Toomre 1972; Gerhard 1981; Negroponte & White 1983; Barnes 1988; Hernquist 1992). We note that the formation of elliptical galaxies from gas-rich mergers at  $z \gg 1$ , and associated star-formation and gas-depletion, would be consistent with their observed old stellar populations.

#### 6.1.2. Collisionless “Dry” Mergers

The isothermal nature of the inner regions of early-type galaxies, already at look-back times of  $\sim 7$  Gyrs, is often explained by a very violent assembly of these regions from collisionless matter, i.e. stars and dark matter (e.g. Lynden-Bell 1967; van Albada 1982; Stiavelli & Bertin 1987). Even though we indeed find isothermal mass density profiles, this is remarkable given the problems with violent relaxation models (e.g. Arad & Lynden-Bell 2005; Arad & Johansson 2005). If we were to consider forma-

tion via mergers of collisionless stellar systems (i.e. “dry mergers”), as suggested by some authors (e.g. Kochfar & Burkert 2003; Nipoti et al. 2003; Boylan-Kolchin et al. 2004; Bell et al. 2005; Naab et al. 2006) we would run into an additional problem. Dehnen (2005) recently showed that the inner cusps of remnants in collisionless merging can *not* be steeper than the cusps of any of the collisionless progenitors and most likely also not more shallow. This invariance seems in agreement with collisionless numerical simulations (e.g. Wechsler et al. 2002; Zhao et al. 2003; Gao et al. 2004; Kazantzidis et al. 2005). The isothermal mass density profile of massive elliptical galaxies would therefore seem to imply that their “dry” progenitors must have had isothermal profiles as well, *ad infinitum*. Clearly this sequence must break down somewhere, if one wants to reconcile our finding with the outcome of cosmological numerical simulations that indicate inner density cusps with logarithmic density slopes around 1.0–1.5 for collisionless mergers (Navarro, Frenk & White 1996; Moore et al. 1998).

### 6.2. Hierarchical Dry Merging of Collisionally Collapsed Gas-rich Progenitors

To bring all the different pieces of evidence for and against gas-poor or gas-rich formation scenarios together and in agreement with the observations from the SLACS and LSD samples, we consider the following scenario:

(1) At a redshift of approximately 1.5 or 2, most of the stellar populations in the inner regions of the massive SLACS/LSD early-type galaxies appear to have been in place already (or was accreted below that redshift through dry mergers), as indicated by their red colors and slow evolution at  $z \lesssim 1$  (Paper II and KT04).

(2) The dominant old stellar population implies that gas accretion and subsequent star-formation can only have played a minor role at lower redshifts (e.g. Trager et al. 2000; Treu et al. 2002). The effect on the inner density slope from adiabatic contraction, resulting from infall of gas-rich satellites, should therefore be relatively small as well. If the latter were important and continued below  $z \sim 1$ , it could severely affect the evolution of the logarithmic density slope, which seems to change at most marginally (§ 4).

(3) Once gas was no longer being accreted, the invariance of the inner density profile (e.g. Dehnen 2005; § 6.1.1) implies that at redshifts above 1.5 or 2, the inner regions of these galaxies were already in dynamical equilibrium (e.g. Wechsler et al. 2002; Zhao et al. 2003; Gao et al. 2004; Kazantzidis et al. 2005). Major or minor collisionless mergers might, however, still occur and replace already present collisionless matter (Gao et al. 2004).

(4) Combining this with the result presented in this paper that the inner cores are very close to isothermal with little intrinsic scatter (§ 3.2; also found by Gerhard et al. 2001 at  $z \approx 0$ ) implies that these cores must have been isothermal already at the time significant gas-accretion ceased to occur at redshifts of 1.5 or 2 or higher.

(5) The results from numerical simulations (e.g. Navarro et al. 1996; Moore et al. 1998), however, suggest that collisionless mergers in a  $\Lambda$ CDM cosmology lead to a much more shallow density profile, never to anything that even remotely resembles an isothermal profile. We

are now faced with a conundrum when trying to explain an isothermal density profile in a dissipationless scenario, whether the merging matter is dark or stellar.

This string of arguments suggests that the isothermal nature of the inner regions of massive early-type galaxies must, somehow, be the result of the effects of gas-accretion (e.g. through mergers) and subsequent (adiabatic) contraction and star formation. During these collisional stages in the galaxy-formation process, the sum of the stellar and dark matter distribution converged to an isothermal density profile through an as yet unknown process. Some of the collisionless matter in the inner regions could be expelled by newly in-falling dark or stellar matter, redistributing it such that the phase-space density remains nearly invariant (e.g. Gao et al. 2004).

This process either occurred rapidly, and only once, for the early-type galaxy in the “monolithic” collapse scenario (e.g. Eggen, Lynden-Bell & Sandage 1962) or in the merging of gas-rich disk galaxies, or it occurred for each of its progenitors, which then hierarchically and collisionlessly merged. Once the gas supply was depleted, subsequent dry mergers would retain the isothermality of the density profile.

The suggested scenario is therefore one where monolithic collapse or gas-rich disk-galaxy merging occurred for the *progenitors* of present-day early-type galaxies (only once in the particular case of the traditional monolithic collapse!) leading to an isothermal density profile. The resulting gas-poor galaxies subsequently merged collisionlessly, leaving the density profiles of the merger products unchanged. Understanding whether this can work, requires detailed numerical calculations, including baryons and feedback in a realistic way. These are only recently becoming available (e.g. Meza et al. 2003; Kobayashi 2005) and still include approximations for many physical processes.

As for observational tests, this hypothetical scenario predicts that the inner regions of massive early-type galaxies already became isothermal (in density) at the formation redshift of the old stellar population. This will be testable if early-type lens galaxies (or their progenitors) are discovered at redshifts of  $z \gtrsim 2$  in future large-scale surveys e.g. with the SKA or the LSST (e.g. Koopmans, Browne & Jackson 2004) and their density profiles can be quantified either through lensing or lensing and dynamics combined.

### 6.3. Open Questions

We end with three open and compelling questions as raised by the results from the SLACS and LSD surveys:

1. *What is the physical process that leads to an average isothermal stellar plus dark-matter density profile in the inner regions of massive early-type galaxies at  $z \gtrsim 1$ ?* The scenario discussed in § 6.2 argues that it most likely is a collisional process.
2. *Why does this process lead to such a remarkably small scatter in the logarithmic (stellar plus dark-matter) density slope in their inner regions?* If collisional processes play a dominant role in this, as suggested above, it requires strong feedback and an attractor-like behaviour. Also, subsequent dry mergers can not increase the scatter significantly



(e.g. Dehnen 2005), suggesting that they have very similar isothermal density profiles.

3. *Why does the mass structure in the inner regions of massive elliptical galaxies evolve so little below a redshift of one?* This suggests that these galaxies are already dynamically in place at  $z \gtrsim 1$  and that the evolution of their mass structure, through subsequent merging, plays only a minor role in their inner regions and must predominantly be dry.

With forthcoming new HST, VLT and Keck data, and improved lensing and dynamical analysis methods, we soon expect to make further progress in answering these questions.

Based on observations made with the NASA/ESA Hubble Space Telescope, obtained at the Space Telescope Science Institute, which is operated by the Association of Universities for Research in Astronomy, Inc.,

under NASA contract NAS 5-26555. Support for program SNAP-10174 was provided by NASA through a grant from the Space Telescope Science Institute, which is operated by the Association of Universities for Research in Astronomy, Inc., under NASA contract NAS 5-26555. The authors are grateful for the scheduling work done by Galina Soutchkova, the Program Coordinator for this HST program. TT acknowledges support from NASA through Hubble Fellowship grant HF-01167.1 and STScI-AR-09222, and thanks UCLA for being such a welcoming and stimulating Hubble Fellowship host institution during the initial phases of this project. The authors acknowledge support from NASA through STScI-AR-09960. The work of LAM was carried out at Jet Propulsion Laboratory, California Institute of Technology, under a contract with NASA. LVEK thanks Oleg Gnedin for useful discussions on adiabatic contraction. The authors thank the referee for helpful suggestions that further improved the paper.

#### REFERENCES

- Abadi, M. G., Navarro, J. F., Steinmetz, M., & Eke, V. R. 2003, *ApJ*, 597, 21
- Abadi, M. G., Navarro, J. F., Steinmetz, M., & Eke, V. R. 2003, *ApJ*, 591, 499
- Arad, I., & Lynden-Bell, D. 2005, *MNRAS*, 361, 385
- Arad, I., & Johansson, P. H. 2005, *MNRAS*, 362, 252
- Arnaboldi, M., et al. 1996, *ApJ*, 472, 145
- Barnes, J. E. 1988, *ApJ*, 331, 699
- Barnes, J. E., & Hernquist, L. E. 1991, *ApJ*, 370, L65
- Barnes, J. E. 1992, *ApJ*, 393, 484
- Barnes, J. E., & Hernquist, L. 1992, *ARA&A*, 30, 705
- Barnes, J. E., & Hernquist, L. 1996, *ApJ*, 471, 115
- Bell, E. F., et al. 2004, *ApJ*, 608, 752
- Bernardi, M., et al. 2003, *AJ*, 125, 1817
- Bertin, G., et al. 1994, *A&A*, 292, 381
- Binney, J. 1978, *MNRAS*, 183, 501
- Binney, J., & Tremaine, S. 1987, Princeton, NJ, Princeton University Press, 1987, 747
- Blumenthal, G. R., Faber, S. M., Primack, J. R., & Rees, M. J. 1984, *Nature*, 311, 517
- Blumenthal, G. R., Faber, S. M., Flores, R., & Primack, J. R. 1986, *ApJ*, 301, 27
- Bolton, A. S., & Burles, S. 2003, *ApJ*, 592, 17
- Bolton, A. S., Burles, S., Schlegel, D. J., Eisenstein, D. J., & Brinkmann, J. 2004, *AJ*, 127, 1860
- Bolton, A. S., Burles, S., Koopmans, L. V. E., Treu, T., & Moustakas, L. A. 2005, *ApJ*, 624, L21
- Bolton, A. S., Burles, S., Koopmans, L. V. E., Treu, T., & Moustakas, L. A. 2006, *ApJ*, in press [Paper I]
- Borriello, A., Salucci, P., & Danese, L. 2003, *MNRAS*, 341, 1109
- Boylan-Kolchin, M., Ma, C.-P., & Quataert, E. 2005, *MNRAS*, 655
- Brinchmann, J., & Ellis, R. S. 2000, *ApJ*, 536, L77
- Bullock, J. S., Kolatt, T. S., Sigad, Y., Somerville, R. S., Kravtsov, A. V., Klypin, A. A., Primack, J. R., & Dekel, A. 2001, *MNRAS*, 321, 559
- Carollo, C. M., de Zeeuw, P. T., van der Marel, R. P., Danziger, I. J., & Qian, E. E. 1995, *ApJ*, 441, L25
- Cohn, J. D., Kochanek, C. S., McLeod, B. A., & Keeton, C. R. 2001, *ApJ*, 554, 1216
- Conselice, C. J., Bershad, M. A., Dickinson, M., & Papovich, C. 2003, *AJ*, 126, 1183
- Dalal, N., & Watson, C. R. 2004, submitted to *ApJ*, astro-ph/0409483
- Dehnen, W. 2005, *MNRAS*, 360, 892
- Dubinski, J. 1994, *ApJ*, 431, 617
- Eggen, O. J., Lynden-Bell, D., & Sandage, A. R. 1962, *ApJ*, 136, 748
- Eisenstein, D. J., Zehavi, I., Nichol, R., Hogg, D. W., Blanton, M. R., Seo, H., Zheng, Z., & Tegmark, M. 2004, *American Astronomical Society Meeting Abstracts*, 205,
- Fabbiano, G. 1989, *ARA&A*, 27, 87
- Fassnacht, C. D., et al. 1999, *AJ*, 117, 658
- Fassnacht, C. D., & Lubin, L. M. 2002, *AJ*, 123, 627
- Fischer, P., Schade, D., & Barrientos, L. F. 1998, *ApJ*, 503, L127
- Franx, M., van Gorkom, J. H., & de Zeeuw, T. 1994, *ApJ*, 436, 642
- Frenk, C. S., White, S. D. M., Efstathiou, G., & Davis, M. 1985, *Nature*, 317, 595
- Frenk, C. S., White, S. D. M., Davis, M., & Efstathiou, G. 1988, *ApJ*, 327, 507
- Gao, L., Loeb, A., Peebles, P. J. E., White, S. D. M., & Jenkins, A. 2004, *ApJ*, 614, 17
- Gebhardt, K., et al. 2003, *ApJ*, 597, 239
- Gerhard, O. E. 1981, *MNRAS*, 197, 179
- Gerhard, O., Kronawitter, A., Saglia, R. P., & Bender, R. 2001, *AJ*, 121, 1936
- Gnedin, O. Y., Kravtsov, A. V., Klypin, A. A., & Nagai, D. 2004, *ApJ*, 616, 16
- Hernquist, L. 1990, *ApJ*, 356, 359
- Hernquist, L. 1992, *ApJ*, 400, 460
- Holz, D. E. 2001, *ApJ*, 556, L71
- Im, M., et al. 2002, *ApJ*, 571, 136
- Jaffe, W. 1983, *MNRAS*, 202, 995
- Jesseit, R., Naab, T., & Burkert, A. 2002, *ApJ*, 571, L89
- Juneau, S., et al. 2005, *ApJ*, 619, L135
- Kauffmann, G., Charlot, S., & White, S. D. M. 1996, *MNRAS*, 283, L117
- Kauffmann, G., & Charlot, S. 1998, *MNRAS*, 297, L23
- Kawata, D., & Gibson, B. K. 2003, *MNRAS*, 346, 135
- Kazantzidis, S., Kravtsov, A. V., Zentner, A. R., Allgood, B., Nagai, D., & Moore, B. 2004, *ApJ*, 611, L73
- Keeton, C. R., Kochanek, C. S., & Seljak, U. 1997, *ApJ*, 482, 604
- Keeton, C. R., & Zabludoff, A. I. 2004, *ApJ*, 612, 660
- Khochfar, S., & Burkert, A. 2003, *ApJ*, 597, L117
- Kochanek, C. S. 1991, *ApJ*, 373, 354
- Kochanek, C. S. 1994, *ApJ*, 436, 56
- Kochanek, C. S. 1995, *ApJ*, 445, 559
- Kochanek, C. S., et al. 2000, *ApJ*, 543, 131
- Kochanek, C. S. 2002, *ApJ*, 578, 25
- Koopmans, L. V. E., & Treu, T. 2002, *ApJ*, 568, L5
- Koopmans, L. V. E., & Treu, T. 2003, *ApJ*, 583, 606
- Koopmans, L. V. E., et al. 2003, *ApJ*, 595, 712
- Koopmans, L. V. E., Treu, T., Fassnacht, C. D., Blandford, R. D., & Surpi, G. 2003, *ApJ*, 599, 70
- Koopmans, L. V. E., Browne, I. W. A., & Jackson, N. J. 2004, *New Astronomy Review*, 48, 1085
- Koopmans, L. V. E. 2004, (Electronic) Proceedings of Science, published by SISSA; Conference: "Baryons in Dark Matter Haloes", Novigrad, Croatia, 5-9 October 2004; editors: R.-J. Dettmar, U. Klein, P. Salucci, PoS(BDMH2004)066
- Koopmans, L. V. E. 2005, *MNRAS*, 363, 1136
- Kormann, R., Schneider, P., & Bartelmann, M. 1994, *A&A*, 284, 285

- Loeb, A., & Peebles, P. J. E. 2003, *ApJ*, 589, 29
- Loewenstein, M., & White, R. E. 1999, *ApJ*, 518, 50
- Lynden-Bell, D. 1967, *MNRAS*, 136, 101
- Ma, C. 2003, *ApJ*, 584, L1
- Matsushita, K., Makishima, K., Ikebe, Y., Rokutanda, E., Yamasaki, N., & Ohashi, T. 1998, *ApJ*, 499, L13
- McIntosh, D. H., et al. 2005, *ApJ*, 632, 191
- Menanteau, F., Jimenez, R., & Matteucci, F. 2001a, *ApJ*, 562, L23
- Menanteau, F., Abraham, R. G., & Ellis, R. S. 2001b, *MNRAS*, 322, 1
- Meza, A., Navarro, J. F., Steinmetz, M., & Eke, V. R. 2003, *ApJ*, 590, 619
- Mihos, J. C., & Hernquist, L. 1996, *ApJ*, 464, 641
- Mo, H. J., Mao, S., & White, S. D. M. 1998, *MNRAS*, 295, 319
- Moore, B., Governato, F., Quinn, T., Stadel, J., & Lake, G. 1998, *ApJ*, 499, L5
- Mould, J. R., Oke, J. B., de Zeeuw, P. T., & Nemec, J. M. 1990, *AJ*, 99, 1823
- Muñoz, J. A., Kochanek, C. S., & Keeton, C. R. 2001, *ApJ*, 558, 657
- Naab, T., Khochfar, S., & Burkert, A. 2006, *ApJ*, 636, L81
- Napolitano, N. R., et al. 2005, *MNRAS*, 357, 691
- Navarro, J. F., & Benz, W. 1991, *ApJ*, 380, 320
- Navarro, J. F., Frenk, C. S., & White, S. D. M. 1996, *ApJ*, 462, 563
- Negroponte, J., & White, S. D. M. 1983, *MNRAS*, 205, 1009
- Nipoti, C., Londrillo, P., & Ciotti, L. 2003, *MNRAS*, 342, 501
- Perlmutter, S., et al. 1999, *ApJ*, 517, 565
- Riess, A. G., et al. 1998, *AJ*, 116, 1009
- Rix, H., de Zeeuw, P. T., Cretton, N., van der Marel, R. P., & Carollo, C. M. 1997, *ApJ*, 488, 702
- Romanowsky, A. J., Douglas, N. G., Arnaboldi, M., Kuijken, K., Merrifield, M. R., Napolitano, N. R., Capaccioli, M., & Freeman, K. C. 2003, *Science*, 301, 1696
- Rusin, D., & Ma, C. 2001, *ApJ*, 549, L33
- Rusin, D., Norbury, M., Biggs, A. D., Marlow, D. R., Jackson, N. J., Browne, I. W. A., Wilkinson, P. N., & Myers, S. T. 2002, *MNRAS*, 330, 205
- Rusin, D., et al. 2003, *ApJ*, 587, 143
- Rusin, D., Kochanek, C. S., & Keeton, C. R. 2003, *ApJ*, 595, 29
- Rusin, D., & Kochanek, C. S. 2005, *ApJ*, 623, 666
- Ryden, B. S., & Gunn, J. E. 1987, *ApJ*, 318, 15
- Saglia, R. P., Bertin, G., & Stiavelli, M. 1992, *ApJ*, 384, 433
- Schneider, P., Ehlers, J., & Falco, E. E. 1992, *Gravitational Lenses*, Springer-Verlag Berlin Heidelberg New York.
- Schweizer, F. 1982, *ApJ*, 252, 455
- Seljak, U. 2002, *MNRAS*, 334, 797
- Sheth, R. K., et al. 2003, *ApJ*, 594, 225
- Spergel, D. N., et al. 2003, *ApJS*, 148, 175
- Stiavelli, M., & Bertin, G. 1987, *MNRAS*, 229, 61
- Tegmark, M., et al. 2004, *Phys. Rev. D*, 69, 103501
- Toomre, A., & Toomre, J. 1972, *ApJ*, 178, 623
- Trager, S. C., Faber, S. M., Worthey, G., & González, J. J. 2000, *AJ*, 120, 165
- Tran, K.-V. H., van Dokkum, P., Franx, M., Illingworth, G. D., Kelson, D. D., & Schreiber, N. M. F. 2005, *ApJ*, 627, L25
- Treu, T., Stiavelli, M., Casertano, S., Møller, P., & Bertin, G. 2002, *ApJ*, 564, L13
- Treu, T., & Koopmans, L. V. E. 2002, *MNRAS*, 337, L6
- Treu, T., & Koopmans, L. V. E. 2002, *ApJ*, 575, 87
- Treu, T., & Koopmans, L. V. E. 2003, *MNRAS*, 343, L29
- Treu, T., & Koopmans, L. V. E. 2004, *ApJ*, 611, 739
- Treu, T., Ellis, R. S., Liao, T. X., & van Dokkum, P. G. 2005a, *ApJ*, 622, L5
- Treu, T., et al. 2005b, *ApJ*, in press
- Treu, T., Koopmans, L.V.E., Bolton, A.S., Burles, S., Moustakas, L.A. 2006, *ApJ*, in press [Paper II]
- van Albada, T. S. 1982, *MNRAS*, 201, 939
- van Dokkum, P. G., Franx, M., Fabricant, D., Kelson, D. D., & Illingworth, G. D. 1999, *ApJ*, 520, L95
- van Dokkum, P. G., & Franx, M. 2001, *ApJ*, 553, 90
- Warren, S. J., & Dye, S. 2003, *ApJ*, 590, 673
- Wechsler, R. H., Bullock, J. S., Primack, J. R., Kravtsov, A. V., & Dekel, A. 2002, *ApJ*, 568, 52
- White, S. D. M., & Frenk, C. S. 1991, *ApJ*, 379, 52
- Winn, J. N., Rusin, D., & Kochanek, C. S. 2003, *ApJ*, 587, 80
- Wucknitz, O. 2002, *MNRAS*, 332, 951
- Wucknitz, O., Biggs, A. D., & Browne, I. W. A. 2004, *MNRAS*, 349, 14
- Zhao, D. H., Mo, H. J., Jing, Y. P., Börner, G. 2003, *MNRAS*, 339, 12

TABLE 1  
LENSING AND DYNAMICAL MODEL RESULTS

Name	$z_l$	$z_s$	$R_e$ ( $''$ )	$\theta_*$ (deg)	$q_*$	$\sigma_{ap}$ ( $\text{km s}^{-1}$ )	$b_{SIE}$ ( $''$ )	$q_{SIE}$	$\theta_{SIE}$ (deg)	$\sigma_{SIE}$ ( $\text{km s}^{-1}$ )	$R_{Einst}$ (kpc)	$M_{Einst}$ ( $10^{10} M_\odot$ )	$f_*$	$\gamma'$
SDSS J0037-0942	0.1955	0.6322	2.38	189.5	0.76	265±10	1.47	0.79	176.2	280	4.77	27.3	0.65±0.19	2.05±0.07
SDSS J0216-0813	0.3317	0.5235	3.37	79.2	0.85	332±23	1.15	0.80	85.0	346	5.49	48.2	0.56±0.16	2.05±0.21
SDSS J0737+3216	0.3223	0.5812	3.26	105.1	0.86	310±15	1.03	0.69	100.5	297	4.83	31.2	0.63±0.20	2.34±0.14
SDSS J0912+0029	0.1642	0.3240	4.81	13.2	0.67	313±12	1.61	0.56	8.7	344	4.55	39.6	0.44±0.13	1.82±0.10
SDSS J0956+5100	0.2405	0.4700	2.60	142.0	0.76	299±16	1.32	0.60	143.4	317	5.02	37.0	0.72±0.21	2.04±0.12
SDSS J0959+0410	0.1260	0.5349	1.82	57.4	0.68	212±12	1.00	0.91	71.6	216	2.25	7.7	0.79±0.23	2.18±0.13
SDSS J1250+0523	0.2318	0.7950	1.77	110.3	0.98	254±14	1.15	0.97	88.7	246	4.26	18.9	1.04±0.30	2.26±0.10
SDSS J1330-0148	0.0808	0.7115	1.23	103.8	0.44	178±9	0.85	0.70	100.0	185	1.30	3.2	1.05±0.30	2.18±0.10
SDSS J1402+6321	0.2046	0.4814	3.14	72.1	0.77	275±15	1.39	0.85	62.2	298	4.66	30.3	0.82±0.23	1.95±0.13
SDSS J1420+6019	0.0629	0.5352	2.60	110.8	0.55	194±5	1.04	0.73	111.7	204	1.27	3.9	1.08±0.31	2.03±0.07
SDSS J1627-0053	0.2076	0.5241	2.14	5.6	0.85	275±12	1.21	0.92	18.7	271	4.11	22.2	1.04±0.30	2.21±0.09
SDSS J1630+4520	0.2479	0.7933	2.02	71.7	0.83	260±16	1.81	0.86	80.8	314	7.03	50.8	0.45±0.13	1.85±0.10
SDSS J2300+0022	0.2285	0.4635	1.80	88.6	0.80	283±18	1.25	0.85	94.3	302	4.56	30.4	0.75±0.22	2.07±0.12
SDSS J2303+1422	0.1553	0.5170	4.20	38.0	0.65	260±15	1.64	0.62	32.5	291	4.41	27.5	0.60±0.17	1.82±0.13
SDSS J2321-0939	0.0819	0.5324	4.47	126.5	0.77	236±7	1.57	0.82	136.2	257	2.43	11.7	0.56±0.16	1.87±0.07

NOTE. — All position angles are defined North to East. The marginalized maximum-likelihood stellar mass fraction ( $f_*$ ) does not include the prior  $f_* \leq 1$ , which ofcourse should be satisfied. We indicated the maximum-likelihood value, as a sanity check to show that none of the systems significantly violates this inequality. Hence the posterior likelihood value, including this prior, is equal to one, if  $f_* > 1$ .